ADVANCED HEALTHCARE MATERIALS
www.advhealthmat.de

Extracellular Matrix-Bioinspired Anisotropic Topographical Cues of Electrospun Nanofibers: A Strategy of Wound Healing through Macrophage Polarization

*Hyeonseo Park,, Tejal V. Patil,, Sayan Deb Dutta,, Jieun Lee,, Keya Ganguly,, Aayushi Randhawa,, Hojin Kim,, and Ki-Taek Lim**

The skin serves as the body's outermost barrier and is the largest organ, providing protection not only to the body but also to various internal organs. Owing to continuous exposure to various external factors, it is susceptible to damage that can range from simple to severe, including serious types of wounds such as burns or chronic wounds. Macrophages play a crucial role in the entire wound-healing process and contribute significantly to skin regeneration. Initially, M1 macrophages infiltrate to phagocytose bacteria, debris, and dead cells in fresh wounds. As tissue repair is activated, M2 macrophages are promoted, reducing inflammation and facilitating restoration of the dermis and epidermis to regenerate the tissue. This suggests that extracellular matrix (ECM) promotes cell adhesion, proliferation, migrationand macrophage polarization. Among the numerous strategies, electrospinning is a versatile technique for obtaining ECM-mimicking structures with anisotropic and isotropic topologies of micro/nanofibers. Various electrospun biomaterials influence macrophage polarization based on their isotropic or anisotropic topologies. Moreover, these fibers possess a high surface-area-to-volume ratio, promoting the effective exchange of vital nutrients and oxygen, which are crucial for cell viability and tissue regeneration. Micro/nanofibers with diverse physical and chemical properties can be tailored to polarize macrophages toward skin regeneration and wound healing, depending on specific requirements. This review describes the significance of micro/nanostructures for activating macrophages and promoting wound healing.

1. Introduction

The skin, which covers the body's surface, is the most significant protective barrier against physical and chemical damage. They can regenerate to some extent when subjected to minor injuries. However, in cases of severe damage where self-regeneration is not possible, more effective treatments are necessary because failure to treat such injuries can lead to mortality.[1,2]

Scaffolds play a fundamental role in numerous applications of regenerative medicine and tissue engineering by providing an optimal matrix for cell growth, proliferation, and differentiation, thereby enabling the restoration and improvement of tissue function. In the field of skin tissue engineering, scaffolds have been extensively researched for their capacity to deliver drugs to wound sites.[3,4] A desirable scaffold for wound healing should possess appropriate physical and mechanical properties, as well as an excellent physiological microenvironment that enables cell adhesion, proliferation, and differentiation. Additionally, the scaffold should exhibit a high degree of porosity, a significant surface-area-to-volume ratio, an interconnected geometric framework, and sufficient flexibility to adapt to the morphology of the wound. Furthermore, scaffolds should maintain a moist environment to facilitate the attachment, proliferation, and migration of cells, stimulate angiogenesis, and promote the formation of new tissue.[5] The morphology and size of the scaffolds are intimately linked to cellular behavior. Hence, the development of scaffolds that emulate the extracellular matrix (ECM) and enable the intricate cellular mechanisms implicated in the creation of new tissue is a primary objective of tissue engineering.[6,7] The composition of the ECM varies among different tissues but typically consists of fibers with diameters ranging from a few micrometers to several hundred nanometers.[8] Nanostructures are characterized by their nanoscale dimensions and are used in tissue engineering to improve their mechanical and biological performance. The small size of nanoparticles rivals that of peptides and small proteins.[9,10] They can easily diffuse across membranes and

H. Park,, T. V. Patil,, S. D. Dutta,, J. Lee,, K. Ganguly,, A. Randhawa,, H. Kim,, K.-T. Lim
Department of Biosystems Engineering
Kangwon National University
Chuncheon 24341, Republic of Korea
E-mail: ktlim@kangwon.ac.kr
H. Park,, T. V. Patil,, J. Lee,, A. Randhawa,, H. Kim,, K.-T. Lim
Interdisciplinary Program in Smart Agriculture
Kangwon National University
Chuncheon 24341, Republic of Korea
S. D. Dutta,, K.-T. Lim
Institute of Forest Science
Kangwon National University
Chuncheon 24341, Republic of Korea
The ORCID identification number(s) for the author(s) of this article can be found under https://doi.org/10.1002/adhm.202304114

DOI: 10.1002/adhm.202304114

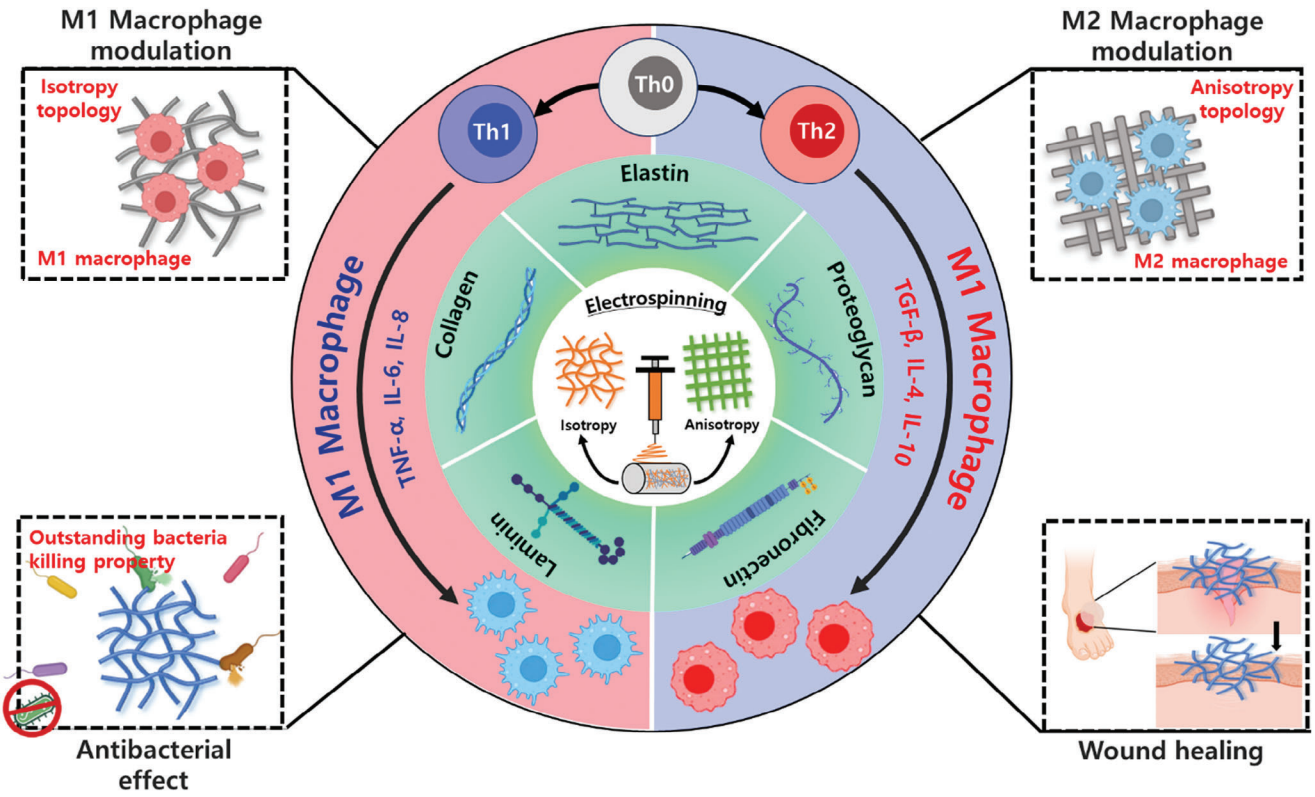

Scheme 1. Schematic representation of utilization of natural biomaterials for electrospun micro/nanofibers and their effect on modulating macrophage polarization toward skin tissue regeneration.

facilitate cellular uptake. Additionally, they can be custom-designed with specific sizes and surface characteristics for various purposes without being limited to predefined sizes.[9] Therefore, the fabrication of nanofiber mats with adjustable diameters using electrospinning is convenient and enables the production of scaffolds that closely mimic the ECM. These electrospun scaffolds have a high potential to promote skin wound healing.[8]

Macrophages are essential immune-regulatory cells that are critical to wound healing. They contribute to wound healing by not only exerting antimicrobial actions and delaying wound closure to eliminate potential pathogens, which can lead to prolonged inflammation and increased scarring but also by resolving inflammation and initiating tissue remodeling and regeneration after pathogen clearance. They modulate the process of wound healing by transitioning from pro-inflammatory (M1-like phenotype) to anti-inflammatory (M2-like phenotype) states.[11,12] Macrophages secrete growth factors such as epidermal growth factor, keratinocyte growth factor, and tumor growth factor-α (TGF-α). These growth factors promote the proliferation of fibroblasts and keratinocytes and the production of collagen and other ECM proteins, promoting granulation and re-epithelialization of the wound. Additionally, macrophages balance the secretion of proangiogenic and antiangiogenic signals to facilitate neovascularization and scar resolution in wounds.[12,13] Macrophages are found throughout all phases of wound healing and are more abundant than other inflammatory cell types. Macrophage depletion can lead to significant alterations in the form of impaired wounds, prolonged healing time, reduced neovascularization, and impaired closure function.[14,15] Alternatively, inappropriate activation of macrophages in fibrotic or chronic non-healing wounds can lead to adverse outcomes.[13] Moreover, if tissue remodeling processes are not effectively controlled, there is a risk of tissue-destructive fibrosis owing to persistent inflammation and maladaptive repair processes.[16] Therefore, fabricating ECM-based scaffolds and nanofibers using biocompatible materials to induce macrophage function is a promising technological approach for promoting wound healing **Scheme 1**.

As shown in the scheme, this review will focus on skin tissue regeneration and summarize and discuss the macrophage response of micro/nano-electrospun fibers with ECM-mimicking anisotropic and isotropic topologies. Herein, we discuss using micro/nanostructures, such as electrospun micro/nanofibers, which significantly activate macrophages and promote wound healing. These structures provide an environment that facilitates the attachment, proliferation, and migration of cells while also influencing the polarization of macrophages toward their regenerative functions.

1.1. Biomolecules in ECM

ECM is a 3D network in animal tissues that supports cells and regulates cellular processes, such as proliferation, adhesion, migration, differentiation, and inflammation.[17,18] Approximately 300 proteins with characteristic domains associated with ECM

have been identified through human genome analysis and DNA sequencing. Supplementary proteins such as growth factors and cytokines also interact with the ECM, initiating enzymatic alterations. The interplay between these elements and the inherent composition of the ECM varies with tissue location, thereby influencing the organization and role of the ECM.[18] The ECM is a vast molecular network composed of collagen, laminin, elastin, fibronectin (FN), and proteoglycans. These components interact with cell adhesion receptors, allowing cells to form complex networks in all tissues and organs.[19] In this section, we discuss the components and the characteristics of each component are outlined below.

Collagen is a major fibrous protein component of the ECM, comprising more than 30% of the ECM. It is characterized by its long, tough, and triple-stranded helical structure. Collagen provides elasticity and stability and serves as a structural material in tissues.[20] In recent studies, it has been documented that there are 28 different types of collagens encoded by over 45 genes present in the tissues and organs of the body.[19,21] Collagen types I, II, and III account for ≈80–90% of the total collagen content in the body.[20] In the initial proliferative phase of wound healing, collagen type III, in conjunction with other ECM molecules like FN and tenascin, establishes a provisional matrix that serves as a substrate for cellular functions. Subsequently, collagen type I becomes the predominant constituent of the ECM, initiating the remodeling stage and the conversion into a more mature extracellular matrix.[22]

Laminin (LM) is a glycoprotein present in the basement membrane, and it demonstrates diverse functionality as a versatile molecule comprising 15 heterotrimeric isoforms.[21] Each molecule is composed of α (400 kDa), β (200 kDa), and γ (200 kDa) chains.[23] They are independently expressed and connected to each other through disulfide bonds at the C-terminal region, forming a cross-shaped asymmetric structure.[21,24] The expression patterns of laminin isoforms vary depending on the spatial and temporal organization of each tissue. The distribution of laminin isoforms shows tissue-specific and cell-specific localization.[20,23] After being formed as a heterotrimer, laminin is secreted into the extracellular space and then interacts with other ECM proteins to form a network. The initial N-terminus (LN domains) exhibit high conservation across isoforms and play a role in the assembly of the molecule through polymerization. The epidermal growth factor-like domains serve as connectors between the globular domains, and they are engaged in various roles such as signaling, growth, and development.[21] Laminin provides structural integrity, contributes to cellular signaling, and performs a pivotal function in biological processes such as cellular adhesion and interaction with collagen and glycosaminoglycans.[21,24]

Elastin is a polymeric protein and a major component of elastic fibers, playing a crucial role in preserving the elasticity and tensile strength of various organs and tissues, including the skin (2–3% dry mass), major arteries and blood vessels (28–32% dry mass), and lungs (3–7%). It is highly deformable, allowing it to withstand repetitive mechanical stress.[25,26] Among them, it is the protein with the highest concentration in the lungs.[27] Elastin provides 1000 times more flexibility than collagen, giving it sufficient mechanical strength for elasticity.[28]

FN is a glycoprotein with a high molecular weight of ≈500 kDa, consisting of two nearly identical subunits that combine to form a dimeric molecule.[19,29] The main function of FN is to facilitate cell adhesion to the extracellular matrix and promote cell migration. The structure of FN is composed of repeating subunits, with a total of 12 FNI (type I), 2 FNII (type II), and 15 FNIII (type III) domains.[21] The FNIII9-10 region of FN contains a synergy binding site (PHSRN) and an RGE binding site, which control the adhesion of integrins. Depending on its molecular structure and splice variants, FN has multiple sequences that allow it to preferentially bind to integrins, collagen, other FN subunits, fibrin, growth factors, and more.[29] FN participates in the wound-healing process through interactions with various cell types and proteins at the site of injury. FN can be categorized into plasma FN and tissue FN based on their spatial expression and distribution. Plasma FN is involved in the formation of fibrinogen and fibrin-FN clots in the bloodstream, aiding the passage of cells like keratinocytes through the temporary matrix of the wound. Tissue FN plays a complex role in ECM remodeling, serves as a necessary component for the deposition of collagen types I and III, and controls the function of lysyl oxidase, an enzyme responsible for the cross-linking of collagen molecules.[22]

Proteoglycan (PG) is a major macromolecule consisting of a core protein and various glycosaminoglycan (GAG) chains. It has a molecular weight of ≈400 kDa.[22,30,31] GAG chains are attached to the proteins classified as PGs, and these GAGs are bound to the peptide chain through O-glycosidic linkage. In addition to the ECM, PGs can also be located on the plasma membrane or within intracellular vesicles. GAG chains located in the extracellular space between cells can retain a significant volume of water and resist external pressure. Therefore, they provide mechanical support to tissue structure and enable cell movement. As a result, PGs play a crucial role in maintaining the structural integrity of the skin.[31] The most common proteoglycans in the skin are decorin and versican.[31] Decorin serves as a binding component of connective tissue, capable of interacting with collagen type I. It plays a crucial role in various cellular processes, such as collagen fiber formation, wound healing, and vascular development.[31,32] The central domain is further divided into two subdomains, GAG-α and GAG-β. Versican is predominantly found in elastic fibers of the skin and influences the generation of elasticity.[31]

2. Wound Healing and Macrophage Function

Wound healing is a complex process involving the movement, differentiation, and proliferation of various cell types in response to intricate signals in the ECM.[33] The stages of wound healing include hemostasis, inflammation, proliferation, and remodeling. Hemostasis can be considered a preparatory stage for the inflammatory phase.[34] Therefore, the final three phases ascertain whether the wound undergoes normal or aberrant healing, marked by the excessive synthesis of ECM proteins and fibrosis.[35]

2.1. Hemostasis

Wound healing involves platelet adhesion to the exposed collagen after tissue damage, coagulation initiation, and blood clot

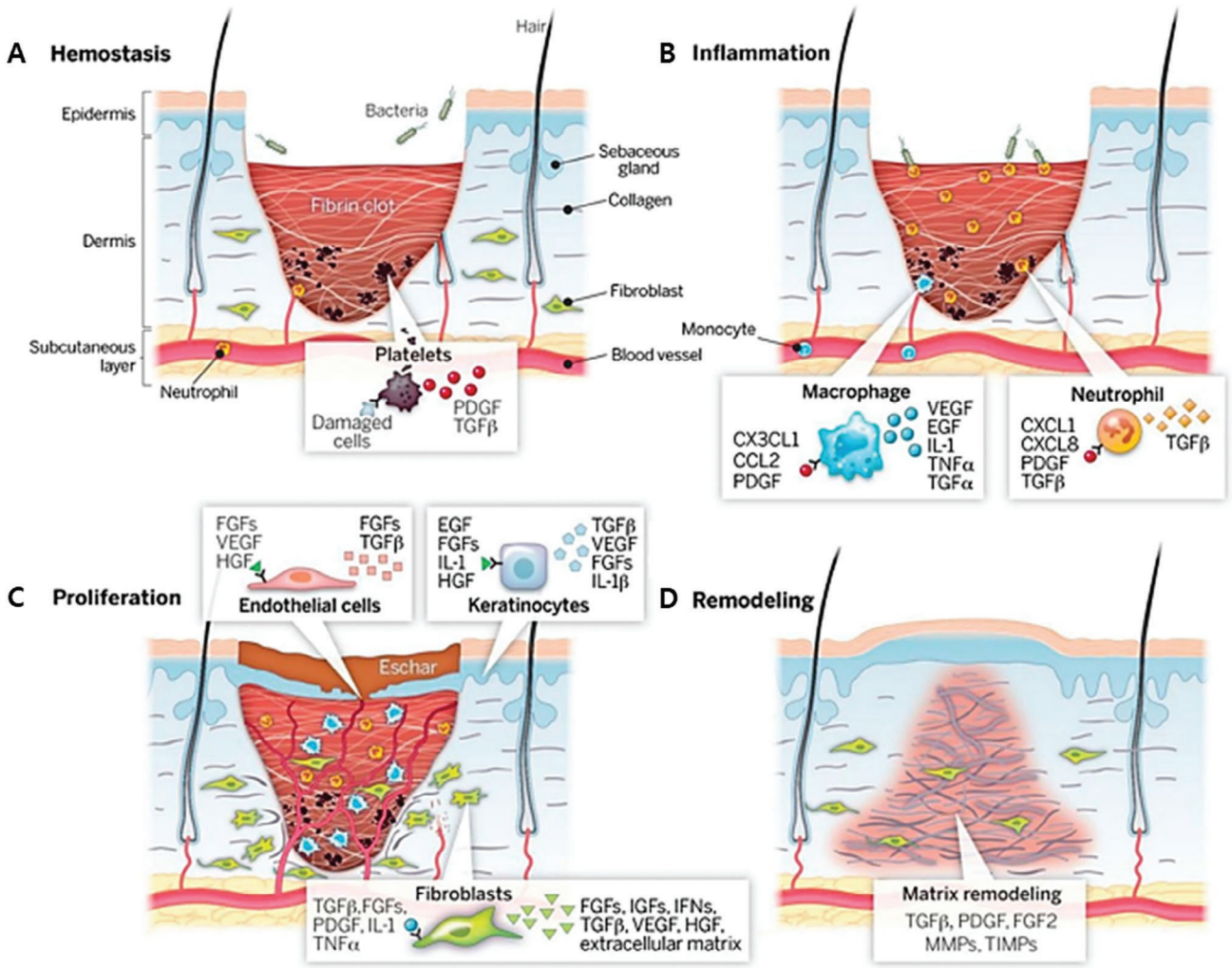

Figure 1. Overview of the macrophage for wound healing process. A) Hemostasis. B) Inflammation. C) Proliferation. D) Remodeling. Reproduced with permission.[37] Copyright 2022, Springer Nature.

formation (**Figure 1A**).[36] Blood clots act as a temporary barrier, aiding skin reconstruction and protecting the wound environment.[37] Upon adhesion of platelets to collagen, the release of adenosine diphosphate (ADP) triggers platelet aggregation. Factor VIII from platelet alpha granules stimulates the formation of a platelet plug, along with the fibrin network, filling the damaged area and creating a transient ECM scaffold for cell migration and proliferation. The fibrin network undergoes rapid plasmin and neutrophil elastase degradation to release sequestered plasma growth factors. Products of fibrin degradation promote ECM deposition, fibroblast proliferation, and angiogenesis. Cell recruitment to the injured tissue relies on the growth factors platelet-derived growth factor (PDGF) and TGF-β, which are crucial for the subsequent inflammatory stage.[36]

2.2. Inflammation

The inflammatory phase, associated with the activation of the innate immune system, begins 24–48 h after wound formation (Figure 1B).[37,38] Injured cells release signals such as damage-associated molecular patterns (DAMPs), hydrogen peroxide (H_2O_2), lipid mediators, and chemokines that attract polymorphonuclear leukocytes (PMNs). PMNs clear microorganisms and debris, releasing cytokines (IL-1β, IL-6, TNF-α) and promoting reparative responses but can also cause injury by releasing proteases and reactive oxygen species (ROS). Macrophages clear PMNs, detect bacteria, and create a microenvironment with elevated ROS and nitrogen species, thereby eliminating bacteria. Macrophages transition into an anti-inflammatory phenotype as DAMPs and pathogen-associated molecular patterns (PAMPs) decrease, preparing them for the next healing phase.[34,39,40]

2.3. Proliferation

Wound-activated keratinocytes respond to mechanical tension, changes in electrical gradients, pathogens, growth factors, and cytokines and undergo a partial epithelial-mesenchymal transition at the wound edge. This transition enhances invasive and

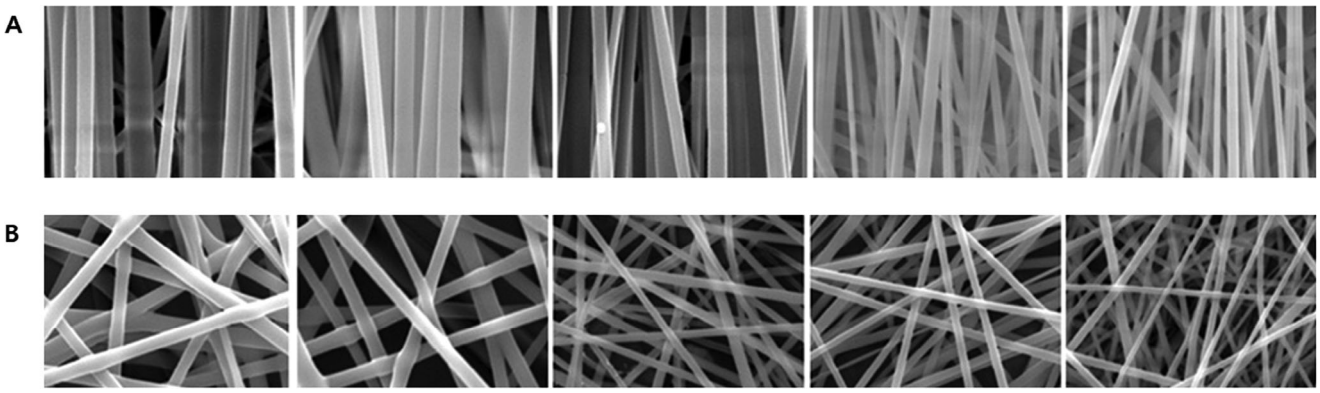

Figure 2. Various morphologies of micro/nanostructures are obtained by electrospinning. A) Anisotropy. B) Isotropy topology. Reproduced with permission.[46] Copyright 2020, American Association for the Advancement of Science.

migratory characteristics. Leading-edge keratinocytes move across the wound and initiate re-epithelialization to restore the epidermal layer. As illustrated in Figure 1C, cells behind the advancing front facilitate cell attachment and realignment with the migrating epithelial layer. Newly formed epidermal keratinocytes secrete matrix metalloproteinases (MMPs) to aid migration and produce new ECM proteins for basement membrane reconstitution. Interactions with structural proteins in the basement matrix guide keratinocytes through the wound-invasion pathway. Granulation tissue formation begins when keratinocytes from opposing edges meet. Granulated tissue serves as a framework for cell migration, supporting neovascularization and ECM deposition. Fibroblasts play a key role in granulation tissue formation and are crucial for generating the fibrous ECM. Macrophages contribute to the fibrotic response by directly influencing fibroblasts, differentiating into myofibroblasts in response to signaling molecules like TGF-β and PDGF.[36,40,41]

2.4. Remodeling

The final stage of wound healing is tissue remodeling, in which macrophages and fibroblasts collaborate to restore the structural integrity. This phase varies in duration (2–3 weeks to over a year) and is influenced by factors such as the wound size and patient condition.[36] This period is dictated by collagen synthesis and decomposition in the ECM. Fibroblasts are crucial for ECM remodeling and replace the initial fibrin clots with hyaluronan, FN, and proteoglycans before synthesizing mature collagen fibrils. Proteoglycans aid collagen organization and cell migration pathways.[41] MMPs degrade collagen type III, which is then replaced by collagen type I (Figure 1D).[36] Apoptosis reduces myofibroblast density, creating fibroblast space, and enhancing ECM mechanical resistance.[38]

During remodeling, macrophages exhibit fibrinolytic and phagocytic traits and secrete proteases to degrade excess fibrotic tissue and phagocytose redundant cells. The failure to resolve excessive cells and matrix in a timely manner can lead to scar formation.[40] Macrophage numbers decrease via apoptosis as the wound heals.[34]

Normal healing outcomes often lack complete integrity and organized structure. After 3 months, a wound typically exhibits 50% of its tensile strength, and the maximum attainable tensile strength of a scar is ≈70–80%.[36]

3. Electrospinning Techniques for Mimicking ECM

3.1. Electrospinning

Electrospinning is a fiber fabrication technique with significant applications in various fields[42]. The standard electrospinning configuration comprises a high-voltage power source, collection apparatus, and syringe pump. When high-voltage direct current is employed by a high-voltage power source, the electrostatic repulsive force exerted on the liquid surface of the polymer solution counteracts the surface tension. Consequently, a droplet of the polymer solution suspended at the end of the spinneret, controlled by a syringe pump, transforms from a semi-spherical shape into a conical droplet known as the Taylor cone. Subsequently, a liquid jet is deposited onto a collector placed at a specific distance, forming nanofibers through deposition.[43] Using electrospinning, various forms of micro/nanostructures can be created. The most representative structures are the anisotropic and isotropic topologies, as illustrated in **Figure 2**. Depending on their isotropic and anisotropic topology, nanofibers have strengths and weaknesses, as shown in **Table 1**. Nanofibers produced by electrospinning exhibit excellent functionality in promoting wound healing.[44] Their microstructures align well with the ECM structure, aiding cell growth, proliferation, and adhesion. Additionally, their exceptional permeability and absorption capacity enable the uptake of wound exudates and maintenance of a moist milieu, fostering an optimized healing environment. Moreover, the expansive surface area facilitates the incorporation and conveyance of bioactive agents such as drugs and growth factors. Consequently, electrospun nanofiber materials can be regarded as an optimal choice for wound dressings.[44]

Biopolymers are natural polymers that are produced by living organisms. A wide range of biopolymers found in plants, including cellulose and lignin, as well as those present in animals, such as collagen, chitin, and chitosan, have diverse applications in biomedicine. Biopolymers are used for drug delivery, tissue engineering, and wound healing. They possess antimicrobial and antiviral properties as well as regenerative potential and biocompatibility. In nanotechnology, biopolymers can be used in pure form

Table 1. Strength and weaknesses of nanofiber structure (↑: increase, ↓: decrease).

	Composites	Strength	Weakness	Application	Reference
Anisotropy	Chlorin e6/silk fibroin	Tensile strength, Young's modulus↑	No degradation study performed and other macrophage phenotypes need to be studied	Macrophage polarization, wound healing	[47]
	Chitosan/poly-ϵ-caprolactone/ Cip	Tensile strength, Young's modulus↑	Cip 2.0% → 5.0%: Cell compatibility↓	Antibacterial property, wound healing	[48]
Isotropy	Silk protein (SF)/polyvinylpyrrolidone (PVP)/puerarin (PUE)	Porosity↑	No degradation, antibacterial study performed	Wound healing	[49]
	Ethanol-soluble polyurethane (EPU)/fluorinated polyurethane (FPU)/thymol	Fiber diameter↑: Hydrophobicity↑	EPU content↑: Tensile stress reduction	Antibacterial property, wound healing	[50]

or mixed with other polymers to create fibrous scaffolds, making them promising candidate materials for skin substitutes.[45]

3.2. Parameters for Electrospinning

3.2.1. Process

The critical voltage varies depending on the polymer used. Only voltages higher than the critical voltage can generate an electrically induced jet from the Taylor cone. Increasing the voltage enhances the electrostatic repulsive force on the jet, allowing for a narrower fiber diameter. Moreover, higher voltages increase the likelihood of bead formation or bead-like nanofibers. The enhanced generation of beads or bead-like nanofibers at higher voltages can be attributed to the reduction in the size of the Taylor cone and the corresponding increase in jet velocity, despite maintaining a constant flow rate. By contrast, at low voltages, the droplet is generally held in suspension at the tip of the needle until the voltage increases, leading to bead-free fiber formation from the Taylor cone.[51,52]

The flow of the polymer solution through the tip of the metal needle governs the structure of the electrospun nanofibers. Uniform and beadless electrospun nanofibers can be produced by maintaining a critical flow rate for the polymer solution. The critical value varies depending on the polymer system used. As shown in **Table 2**, increasing the flow rate beyond the critical value allows for surface formation. However, increasing the flow rate beyond the critical value results in a shorter drying time before reaching the collector and lower stretching forces, leading to an increase in the pore size and diameter of the nanofibers, as well as the formation of distorted Taylor cones and more droplets. Both increases and decreases in the flow rate can influence the nanofiber formation and diameter; therefore, maintaining a minimum flow rate is preferred to balance the detachment of the polymer solution and its replacement with a fresh solution during jet formation. In addition, a low flow rate is recommended to ensure that the polymer solution has sufficient time for polarization. This allows for the formation of a jet cone and a retraction jet (a jet formed directly from within the needle without droplets or cones). The retraction jets are unstable and constantly transition to cone jets during electrospinning. This dynamic phenomenon leads to the formation of nanofibers with varying diameters.[51–53]

The distance between the collector and needle tip plays an important role in determining the morphology of the electrospun nanofibers. The fiber morphology is easily influenced by factors such as the precipitation time, evaporation rate, bending, and instability, making the distance critical. Therefore, to achieve smooth and uniform electrospun nanofibers, it is important to maintain a critical distance; variations on both sides of this distance can affect the fiber morphology. As shown in Table 2, when the distance between the collector and needle tip is small, the emitted jet of the solution does not have sufficient time to bend or whip, resulting in defective nanofibers with larger diameters. Conversely, as the distance increases, the polymer solution jet can bend and whip more, reducing the fiber diameter. This is one of the reasons why the fiber diameter decreases in electrospinning.[51,54]

3.2.2. Polymer

Molecular Weight: The molecular weight of a polymer influences its properties, such as the glass transition temperature, melting point, mechanical strength, and solubility. An appropriate molecular weight is necessary for successful fiber formation. Otherwise, it may lead to electrostatic spraying and the inability to obtain fibers. There are minimum concentrations that stabilize the fiber structure and maximum concentrations where electrospinning is not possible for each molecular weight. The diameter of the resulting fibers tends to increase with increasing relative molecular weight of the polymer, and the spacing between fibers also increases. Additionally, as the molecular weight increases, the entanglement of polymer chains intensifies, and the bead structure reduces.[55–57]

Solvent: Before selecting a solvent, two considerations should be taken into account. Firstly, the solvent used in the electrospinning process should include polymers that are completely soluble in it (Table 2). Secondly, it should have an appropriate boiling point.[51] Solvents with exceedingly high or low boiling points are not conducive to the electrospinning process. As indicated in Table 2, solvents with low boiling points can clog the nozzle and disrupt the fiber formation process, while solvents with high boiling points are not ideal for promoting the solidification of polymer fibers during electrospinning. By adjusting the solvent

Table 2. Electrospinning process parameters (↑ high, increase; ↓ low, decrease).

Parameters		Properties	References
Process	Voltage	↑: Diameter ↓, bead and bead nanofibers↑	[51, 52]
		↓: Drop hangs from needle end until voltage increases	
	Flow rate	Low flow rate recommended	[51–53]
		↑: Surface formation, pore size and diameter of the fiber↑, distorted Taylor cone, large amount of drops	
	Distance between collector and needle tip	↓: Defective nanofibers with larger diameters	[51, 54]
		↑: Diameter ↓	
Polymer	Molecular weight	Appropriate: fibrosis progresses well	[55–57]
		↑: Diameter and spacing between fibers ↑, bead structure↓	
	Solvent	Need a polymer that is completely soluble	[51, 55, 58]
		-boiling point	
		↑: Not suitable for promoting coagulation of polymer fibers	
		↓: Obstructing the fibrosis process	
Solution	Conductivity	↑: Diameter ↓, formation of the multiple jets and the protrusions in the fibers	[51, 59, 60]
		↓: Electrospinning impossible	
	Viscosity	↑: Results in fewer beads	[61, 62]
		↓: Intermittent bead occurs	
	Surface tension	↑: Bead formation, prevents fiber formation, transform into water droplets	[52, 62–64]
		↓: Bead fiber → soft fiber	
Environmental	Humidity	↑: Thinner nanofibers formed	[51, 65]
		↓: Thicker nanofibers formed	
	Temperature	↑: Diameter ↓	[62, 66]
		↑: Electrical suspension of elongation	

system through solvent blending, it is possible to manufacture unique fiber structures with various surface roughness, porosity, and flat cross-sections.[55] In addition, solvents can be used to produce highly porous nanofibers, which can occur when polymers are dissolved in two different solvents, one of which acts as a nonsolvent. The difference in evaporation rates between the solvent and nonsolvent leads to phase separation, resulting in the production of highly porous nanofibers.[51] Currently, halogenated solvents (e.g., chloroform, trifluoroethanol) and toxic solvents (e.g., dimethylformamide) are commonly used in the field of electrospinning.[58]

3.2.3. Solution Properties

The conductivity of the solution not only affects the formation of the Taylor cone but also has an impact on the regulation of nanofiber diameter. In polymer solutions with very low conductivity, there is no surface charge present on the fluid droplet surface to facilitate the formation of the Taylor cone, making electrospinning impossible. On the other hand, as the conductivity increases, the surface charge on the solution surface also increases, contributing to the formation of the Taylor cone and simultaneously reducing the average diameter of the fibers, which is related to the power law relationship. However, the jet current initially increases but then exhibits a decreasing trend. These phenomena can be explained by the variations in surface charge distribution around the electrospun jet and changes in the tangential electric field along the fluid surface. Another phenomenon observed when the conductivity of polymer solutions increases is the formation of multiple jets and the occurrence of bead protrusions in the fibers (Table 2).[51,59] In addition, the charge-carrying capacity of the solution also influences the process. As the conductivity of the solution increases, more charge can be carried, resulting in an increase in the length of the polymer jet under a high electric field.[60] The electrical conductivity of a polymer solution can be

regulated by incorporating a suitable salt. The inclusion of salt influences the electrospinning process in two ways. Firstly, it increases the number of ions in the polymer solution, leading to an increase in the surface charge density of the fluid and the electrostatic forces generated by the external electric field. Secondly, it increases the conductivity of the polymer solution, reducing the electric field directed along the fluid surface. However, if the conductivity of the solution increases too much, this electric field reduction can decrease the electrostatic forces acting along the fluid surface, negatively affecting the formation of the Taylor cone.[51]

The viscosity of a solution is influenced by the concentration of the polymer solution, the surrounding temperature, the molecular weight of the polymer, and the impurities present in the solution. Therefore, it is possible to control the viscosity by adjusting the temperature or molecular weight. The relationship between molecular weight and viscosity is described by the Mark–Houwink–Sakurada equation (Equation (1)).

$$[\eta] = KM^{a} \tag{1}$$

In this equation, η represents viscosity, M is the molecular weight, and K and a are the Mark–Houwink parameters or empirical constant parameters. The values of the Mark–Houwink parameters vary depending on the polymer-solvent system. In Table 2, if the viscosity of the polymer solution is too low, intermittent beads can occur in the resulting nanofiber structure. On the other hand, increasing the concentration of the polymer solution results in an increase in the entanglement between polymer chains, leading to an increase in viscosity. This higher viscosity reduces the occurrence of beads in the solution. The diameter of the fibers is related to the diameter and spacing of the beads, and a thinner fiber corresponds to a closer distance between the beads. Therefore, to obtain consistent fibers, it is important to maintain a constant viscosity of the solution.[61,62]

Surface tension refers to the cohesive forces between molecules within a liquid, which is influenced by intermolecular interactions.[63] Surface tension determines the upper and lower limits of the range in which electrospinning can be achieved.[64] If the surface tension is too high, fibers cannot be formed and instead transform into droplets (a process known as electrospraying). Generally, surface tension is overcome by the electric field to generate a polymer solution jet. As mentioned in Table 2, high surface tension promotes bead formation. Beads possess a higher ratio of surface area to volume in comparison to fibers, which leads to reduced surface energy remaining on their surface.[62] On the contrary, if the surface tension is low, bead fibers can be transformed into smooth fibers. Lower surface tension allows for the formation of smoother fibers with reduced bead formation.[52] The surface tension in polymer solutions can be adjusted by controlling the polymer/solvent ratio. Another method is to add a surfactant to the solution, which provides uniformity to the fibers.[64]

3.2.4. Environmental Factors

Humidity can modulate the diameter of nanofibers by regulating the solidification mechanism of the charged jet. Lower relative humidity accelerates solvent evaporation, leading to the formation of thicker nanofibers. Conversely, higher humidity suppresses solvent evaporation, resulting in thinner nanofibers. Additionally, humidity also influences the formation of pores in the nanofibers (Table 2). This phenomenon is known as the "breath figure," which refers to the fog-forming process occurring when water vapor contacts a cold surface. When the polymer solution moves toward the collector, the condensation of water vapor occurs, forming water droplets that leave traces as they dry, creating pores in the polymer structure.[51,65]

The electrospinning process at high temperatures reduces the viscosity, surface tension, and conductivity of the polymer solution. These factors contribute to the effective application of electrical forces for generating fibers with small diameters. However, at high temperatures, the viscosity of the polymer solution decreases due to faster solvent evaporation compared to ambient conditions. This premature solvent evaporation can lead to the premature termination of the electrical stretching process (Table 2).[62,66]

4. Materials for Fabrication of Micro/Nanofibers

4.1. Natural Materials

Micro/nanofibers possess physical characteristics and surface properties that can enhance their hemostatic properties and potentially replace adjunctive hemostatic agents. The mesh-like structure of the fibers is ideal for exudate removal from wounds and can absorb water within a range of 18–213%, depending on the material. Moreover, they can maintain a moist environment conducive to cellular respiration, survival, and proliferation, promoting wound healing and closure and preventing scar formation. Matrices with high porosity allow gas to permeate the membranes and protect tissues from dehydration. Additionally, they can serve as drug carriers, enabling the release and delivery of drugs to wound dressings. Their high flexibility allows for rapid adaptation to wound contours, eliminating the need for secondary dressings for stabilization.[67] Some naturally available biomaterials, such as collagen, gelatin, laminin, elastin, GAG, and decellularized ECM, with their respective potential in the fabrication of micro/nanocomposites and cell behavior, are described below and listed in **Table 3**.

Collagen is widely used as a skin substitute and wound dressing because of its hemostatic and cell-proliferative effects on fibroblasts and keratinocytes.[68] Collagen dressings have a high absorbency capacity, allowing them to absorb a significant amount of exudate and reduce protein and electrolyte loss caused by traumatic exudates. They also help to prevent wound dehydration.[69] However, collagen extracted from animal tissues undergoes denaturation during electrospinning, which results in weakened mechanical properties and higher degradation rates.[70] Additionally, collagen is easily soluble in water, and its rapid degradation can lead to the disappearance of the scaffold before the cells can deposit their own ECM.[71] Therefore, modifications are necessary to enhance the mechanical strength.[69] Crosslinking is one of the methods used to enhance the mechanical strength of collagen. Collagen can undergo chemical crosslinking (e.g., with glutaraldehyde, genipin, and carbodiimides), enzymatic crosslinking (e.g., with transglutaminase, tyrosinase, and laccase), or physical crosslinking (e.g.,

Table 3. Natural materials function and application in skin tissue regeneration.

Natural materials	Function	Composites	Highlight	References
Collagen	Effects of blood clotting and cell proliferation in fibroblasts and keratinocytes, possesses strong absorbency, absorbs a large amount of secretion	Ethyl cellulose, poly lactic acid, silver sulfadiazine (AgSD)	NIH 3T3 cell attached well to the surface (for 7 days)	[88]
		PVA, gelatin, alginate	Cell proliferation (after 3 days): Better than non-collagen injected scaffolds	[89]
		PCL, N-acetylcysteine	Percentage of wound closure area: 93.59% (12^{th} day)	[90]
Gelatin	Hemostatic properties, excellent biocompatibility, reduced cytotoxicity, low antigenicity, controllable biodegradability, ability to stimulate cell attachment and growth	PCL, cellulose nanocrystals	Wound closure area percentage: 98 ± 3% (14th day)	[91]
		PCL, zinc oxide nanoparticles	Complete formation of the epidermis (at day 13)	[92]
		PLCL, epigallocathechin-3-Ogallate	Antioxidant, antibacterial, wound healing, cell differentiation	[93]
Elastin	Providing mechanical elasticity, gradually reducing wound contraction, enhancing re-epithelialization	Collagen, glutaraldehyde	Wound contraction rate: 50.7% (28^{th} day)	[94]
		Collagen, carbonyldiimidazole	High growth rates of human keratinocytes and fibroblasts	[95]
		Chitosan, magnesium phosphate	Elongated morphology of cells on elastin added nanofibers	[96]
Hyaluronic acid	Promote cell proliferation and movement by maintaining moisture balance in the wound area, providing nourishment, cleansing infected wound areas.	Poly (ethylene oxide)	Cell activity of the extract of the L929 cells (for 72 h): 1.33 ± 0.039nm	[97]
		ZnO, cinnamon essential oil	Complete suture of wound (day 17)	[98]
		Chitosan, PCL	Improved cell spreading and proliferation (after 5 days)	[99]

with UV radiation, gamma radiation, and dehydrothermal treatment). In addition, incorporating synthetic polymers into composite nanofibers can improve their mechanical and biological properties.[71] For example, Li et al. developed poly-ϵ-caprolactone (PCL)-Col/ZnO-0.75 + vascular endothelial growth factor (VEGF) fibrous scaffolds and photographed them from the day of implantation until the wounds completely healed (**Figure 3**A–a). On the fourth day, as shown in **Figure 3**A–b, the percentage of the wound area treated with PCL-Col/ZnO-0.75 + VEGF was 66%, which decreased to ≈22% and 3% after 6 and 12 days of treatment, respectively. This indicates that the PCL-Col/ZnO-0.75 + VEGF fibrous scaffold significantly promotes wound healing.[72]

Similarly, gelatin, a protein obtained from partial hydrolysis of animal collagen, exhibits hemostatic characteristics, remarkable biocompatibility, reduced cytotoxicity, minimal antigenicity, adjustable biodegradability, and the ability to promote cellular adhesion and proliferation (Table 3). Because of these properties, they are extensively utilized in human applications, specifically in wound dressings and tissue engineering products. Porous gelatin matrices maintain a moist environment by absorbing the wound exudates, thereby promoting wound healing. Additionally, this matrix acts as a porous scaffold for cell migration, providing structural and mechanical support and facilitating the growth of new tissues. However, the electrospinning ability of gelatin is low.[73] Nanofibers of pure gelatin typically have a random coil conformation, resulting in poor water resistance and mechanical properties. This leads to immediate dissolution upon contact with water. Various physical and chemical crosslinking methods have been developed to address these issues. Physical cross-linking methods are primarily based on physical forces, including hydrogen bonding, polar bonding, electrostatic interactions, and van der Waals forces. Crosslinking can enhance the water resistance. Chemical crosslinking can impart a more stable crosslinked network to gelatin nanofibers than physical crosslinking. Chemical cross-linkers include formaldehyde, glutaraldehyde, isocyanates, acrylamides, and epoxides.[74] Chemically crosslinked nanofiber mats exhibit ten times higher elongation at break and ultimate tensile strength than uncrosslinked nanofiber mats.[75]

Laminin (LM)-derived peptides are peptide sequences derived from the LM protein that can be coated onto the surface of a substrate to facilitate cell adhesion. These peptides were found to promote uniform cell proliferation and enhance cell adhesion and spreading compared with substrates without LM-derived peptides.[76] LM plays a significant role in adult skin, with major isoforms such as LM-332, LM-311, and LM-511, predominantly produced by keratinocytes. LM-511 stabilizes epidermal adhesion, mediates epidermal-dermal communication, and promotes skin regeneration. It also plays a crucial role in re-epithelialization and neovascularization during wound healing. The cell compatibility of LM is not limited to keratinocytes but is a general characteristic of various cell types, including skin

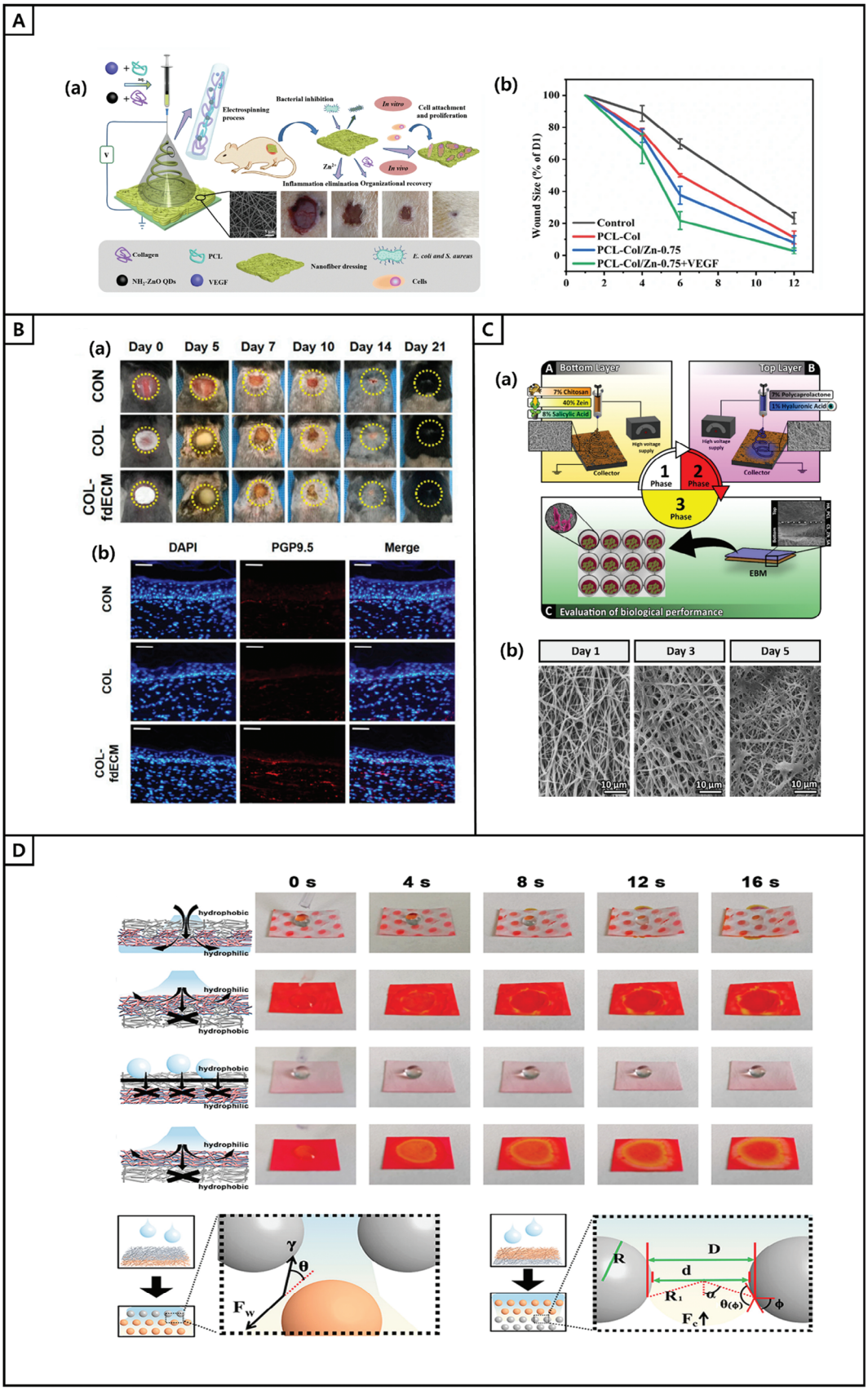

and epidermal cells. Moreover, numerous heparin-binding domains (HBDs) within the LM can serve as reservoirs for growth factors, enhancing their biological activity. The preservation of growth factors can be improved by incorporating HBDs into the fibrin matrix through covalent binding within LM. This approach specifically augments the impact of growth factors, such as PDGF and VEGF, thereby facilitating wound healing in vivo.[77] LM nanofibers created by blending various synthetic polymers, such as polylactic acid (PLA)/ poly lactide-co- glycolic acid (PLGA) and polycaprolactone, can enhance cell adhesion to synthetic biomaterials.[76]

Elastin, a key ECM protein, provides mechanical elasticity and interacts with cells to progressively reduce wound contraction and enhance dermal regeneration, contributing to wound healing (Table 3).[78] Elastin can be blended with various natural and synthetic polymers such as PLGA, silk, poly (3-caprolactone), and collagen to enhance the physicochemical and mechanical properties of biomaterials via electrospinning.[76] However, in cases of severe skin damage, insufficient elastin is produced.[79] Furthermore, considering that the elastic fiber network in the skin is primarily formed during early life and is minimally replenished in adulthood, it is difficult to recover if the network is compromised using tropoelastin. Tropoelastin is a major component and building block of elastic fibers. Recombinant human tropoelastin serves as a matrix for skin fibroblasts, promoting collagen synthesis and glycosaminoglycan deposition, thereby contributing to tissue regeneration and improving skin hydration. Additionally, it can provide clinically meaningful insights into the functional role of elastin in the ECM and offer opportunities to improve wound healing and reduce scar formation.[78]

When a wound occurs, a provisional ECM composed of fibrin and FN is initially formed and later replaced by a mature ECM with a higher FN content. FN plays crucial roles in various processes related to cell adhesion, contraction, migration, differentiation, gene expression, and angiogenesis. Therefore, FN is an essential component for ECM formation, re-epithelialization, and tissue regeneration, indicating the potential of FN-based nanofibers in wound healing devices. However, the production of FN nanofibers does not fully replicate the natural pattern of FN fiber formation.[68] Therefore, FN is primarily used for coating polymer fibers to enhance their biocompatibility and cell adhesion properties. It is combined with various synthetic and natural materials to explore potential tissue engineering applications.[76]

Glycosaminoglycans (GAG) play a crucial role in skin tissue regeneration and various stages of maturation. They interact with growth factors to effectively promote cell proliferation.[80] During the proliferative phase of wound healing, GAG-peptide fragments released from the wound due to protease-mediated proteoglycan (PG) degradation can bind to positive proteins (e.g., elastase and cathepsin G) and inhibit their respective activities. They also interact with various protein-degrading enzymes, thereby enhancing their activities.[77] During the remodeling phase, restoration of vascular density in the wound area is supported by capillary growth, FN deposition, and collagen formation. Hyaluronic acid (HA), is another interesting material that plays an active role in all stages of wound healing and regulates innate immune responses to tissue remodeling and tissue damage.[67] This is because it is a hygroscopic polymer that helps maintain the moisture balance at the wound site, thereby promoting cell proliferation and migration (Table 3).[81] In addition, it forms a temporary matrix in the early stages of wound formation, providing nutrition and helping to cleanse the infected wound site (Table 3).[82] However, electrospinning of pure HA can pose challenges depending on the characteristics of the HA solution and the electrospinning apparatus used. One of the main issues is the high viscosity of HA solution owing to the long-range electrostatic interactions arising from its ionic nature. The presence of counter-ions in the solution increased the viscosity of HA. High viscosity prevents effective interactions between HA polymer chains, leading to instability in the jet and the production of discontinuous and heterogeneous fibers. Additionally, HA solutions may result in droplets or spatters between the collector and needle because of their inability to evaporate in the collection space. To facilitate the electrospinning of HA, it is possible to mix HA with suitable polymer materials or use solvent blends that modify the surface tension and viscosity of HA by altering the helical structure within HA chains and intra-molecular hydrogen bonding.[67]

The cellular contents of the ECM can be removed, resulting in the conversion of the ECM to decellularized ECM (dECM). Recent studies have shown that the dECM plays a crucial role in skin wound healing.[83] This is because dECM possesses a unique microstructure, abundant bioactive molecules, and a specific chemical composition that can influence cell proliferation, migration, and differentiation.[84] Additionally, dECM exhibits various biological origins and favorable biocompatibility and biodegradability.[85] Moreover, the composition and microenvironment of dECM closely mimic the natural ECM, providing cells with a microenvironment that includes ECM components.[76] Some dECM scaffolds have low mechanical strength, which poses a challenge when long-term mechanical support for regenerating tissues is required, particularly for treating large defects in load-bearing tissues. One strategy for addressing this constraint is to employ electrospinning to combine dECM scaffolds with synthetic biocompatible polymers. These hybrid scaffolds can provide mechanical support structures while preserving the biological activity of the dECM, offering significant advantages for tissue engineering and regenerative medicine applications.[86] All of these materials can be used in the fabrication of micro/nanocomposites after blending with synthetic polymers which have the potential to produce nanofibers using electrospinning. For example, Kim et al. added a fibroblast-derived ECM (fdECM) to collagen I to create a patch. They applied this patch to a skin wound model to confirm its

Figure 3. A–a) Schematic diagram of PCL/Col/Zno+VEGF scaffold for wound healing. b) Wound closure rate of each group. Reproduced with permission.[72] Copyright 2021, Springer Nature. B–a) Evaluation of wound healing for CON, COL, and COL-fdECM scaffolds. b) Immunofluorescent images of each scaffold stained with PGP9.5 (in red). Reproduced with permission.[87] Copyright 2022, Frontiers. C–a) Schematic of the steps in EBM fabrication. b) SEM images for evaluating bacterial growth on the surface of EBM samples. Reproduced with permission.[100] Copyright 2016, Elsevier B.V. D) Unidirectional automatic liquid removal capability and contact-pumping mechanism of nanofiber dressing. Reproduced with permission.[101] Copyright 2022, American Chemical Society.

Table 4. Synthetic materials function and application in skin tissue regeneration.

Synthetic materials	Function	Composes	Application	References
PCL	High biocompatibility, low melting point, glass transition temperature	Chitosan, curcumin	Methicillin-resistant *Staphylococcus aureus* (MRSA) infected wound healing percentage (day 10): 96.25%, 98.5% (respectively MRSA treated and untreated wounds)	[111]
		Zinc oxide	More than 60% of the wounds were completely healed	[112]
		Curcumin, silk fibroin, PVA	Wound healing rate (on day 12): 96.75%	[113]
PLA	Biocompatibility, biodegradability, excellent thermal and mechanical properties and processability	Curcumin, polyethylene glycol (PEG)	Satisfactory cell attachment to nanofibers	[114]
		PVA, sodium alginate	Wound healing rate (on day 16): Almost complete healing	[115]
		Triterpene extract (TE)	Drug delivery more than 60% of TE is released in 0.5 h	[116]
PVA	Biocompatibility, biodegradability, superior transparency, film-forming abilities, thermal stability, chemical resistance	Silk fibroin	Wound closure (at day 5): 1.35 fold ↑(compared with control group)	[117]
		Chitosan-stabilized Prussian blue	Excellent cell proliferation, antioxidant	[118]
		Gum Arabic, silver nanoparticles	Mouse embryonic fibroblast (MEFs) cell: Substantial increase (on day 5)	[119]
PLGA	Controlled and sustained release properties, low toxicity, biocompatibility with tissues and cells	Vildagliptin	Wound healing percentage (on day 14): 11.4 ± 3.0%	[120]
		Insulin, vildagliptin	Wound region size (on day 14): 1.9 ± 0.3 mm	[121]
		Curcumin, heparin	Wound size: Less than 14% compared to original size (within 14 days)	[122]

wound-healing effect. As shown in Figure 3B–a, after 14 days, in the control group (CON) where nothing was applied, there was an exudate with blood on the skin. In contrast, in the control collagen patch (COL) and fdECM-collagen patch (COL-fdECM) groups, the wounds were almost completely epithelialized. In particular, the wound area was smaller in the COL-fdECM group. Additionally, when confirming whether the severed nerve fibers were reinnervated from the nerve ganglia to the skin, the COL-fdECM group showed a higher area of PGP9.5-positive nerve fibers in the superficial dermis than the other groups. These results suggest that fdECM assists in reconstructing skin wounds back to the original tissue (Figure 3B–b).[87]

4.2. Synthetic Materials for Fabrication

Synthetic biocompatible polymers have significant potential in the applications of skin tissue engineering and wound dressings, providing a controlled release of bioactive molecules and supporting the regeneration of healthy skin tissue. The commonly used synthetic degradable polymers in electrospinning for these purposes are poly-ϵ-caprolactone (PCL), polylactic acid (PLA), polyvinyl alcohol (PVA), and poly lactide-co-glycolic acid (PLGA). Each of these polymers is briefly discussed below.

PCL is a biocompatible, non-toxic, and biodegradable polyester. It is an ideal material for manufacturing nanofibers using the electrospinning technique, providing high biocompatibility (**Table 4**).[102] Furthermore, PCL is a polymer with a low melting point and glass transition temperature (Table 4). It exhibits excellent solubility in organic solvents such as hexafluoroisopropanol, dichloromethane, chloroform, methanol, and tetrahydrofuran. This property makes it highly suitable for applications where longer degradation times are desired. When PCL is composed of more hydrophilic monomers, it promotes faster water diffusion, thereby increasing the degradation rate.[103] However, PCL has lower surface solubility compared to PLA and PLGA, resulting in reduced cell adhesion. Therefore, PCL is typically used in combination with other polymers and bioactive

additives rather than being electrospun alone.[104] Figueira et al. conducted a study on tissue regeneration and fabricated a bilayer nanofibrous membrane, referred to as an electrospun bilayer membrane (EBM), using the electrospinning technique. The upper layer of the EBM consisted of polycaprolactone (PCL) and hyaluronic acid (HA), while the bottom layer was composed of chitosan (CS) and zein. To impart anti-inflammatory and antimicrobial activity, salicylic acid (SA) was incorporated into the membrane (Figure 3C–a). The antimicrobial activity of EBM was evaluated using the *Staphylococcus aureus* strain, and the biofilm formation on the membrane surface was analyzed by SEM over a 5-day period. The results demonstrated that EBM generated an inhibitory zone with a diameter of 9.84 ± 3.64 mm. Furthermore, even after 5 days, no biofilm formation was observed on the surface of EBM (Figure 3C–b). This result is interpreted as the combined effect of CS and SA, both possessing antimicrobial properties in the bottom layer of EBM. These characteristics suggest a positive impact on wound healing.[100]

PLA is an aliphatic polyester that can be synthesized from sustainable and renewable sources. It is considered one of the most promising biopolymers in biomedical applications due to its biocompatibility, biodegradability, excellent thermal and mechanical properties, and processability. The advantages and examples of PLA are shown in Table 4. In particular, electrospun PLA nanofibers, with their similarity to the ECM, large surface area, high porosity, small pore size, and diverse mechanical properties for various applications, have recently gained significant attention and impact.[105] Furthermore, electrospun PLA nanofibers also hold great potential as drug delivery carriers in addition to being scaffolds for tissue regeneration. They offer a wide range of applications in the field of drug delivery.[106] However, PLA has some drawbacks, such as a low melting point and slow crystallization rate. These limitations can be overcome by blending PLA with other polymers or substances similar to other materials.[103] For example, Zhang et al. fabricated Janus nanofibers with an upper layer composed of polyacrylonitrile (PAN) containing phenol red (PSP) and a lower layer consisting of polylactic acid (PLA) containing encapsulated oxacillin (OXA) and polyoxometalate (P2W18). These nanofibers exhibited a pattern with 3 mm hole sizes, enabling complete drainage of water droplets from the hydrophobic layer to the hydrophilic layer (Figure 3D). When a water droplet contacted the hydrophobic layer, it was rapidly expelled, whereas it was blocked when it touched the hydrophilic layer. These results indicate that the nanofibers possess the ability to unidirectionally expel water, making them effective for wound management.[101]

PVA is one of the earliest synthetic polymers and is categorized as a water-soluble synthetic polymer. It is widely used in advanced biomedical applications due to its excellent biocompatibility, biodegradability, superior transparency, film-forming abilities, thermal stability, and chemical resistance (Table 4). PVA can be electrospuned to form high-quality nanofibers. However, its application is limited by its relatively low strength, poor thermal stability, and immediate dissolution or excessive swelling in aqueous environments. Therefore, to enhance its mechanical properties and water resistance, the cross-linking process becomes essential.[107,108] Cross-linking of PVA can be achieved through various chemical reactions, such as free-radical polymerization, chemical reactions of complementary groups, high-energy irradiation, or enzymatic reactions. It can also undergo cross-linking through physical reactions, including ionic interactions, crystallization of the polymeric chain, hydrogen bonding, protein interactions, or the design of graft copolymers. The most commonly used chemical agents or crosslinkers for PVA are dialdehydes, diisocyanates, dicarboxylic acids, tricarboxylic acids, and boric acids.[107]

PLGA is a biodegradable polymer synthesized by the ring-opening co-polymerization of lactic acid and glycolic acid monomers.[104] Lactic acid is rigid, highly hydrophobic, and slowly degradable, while glycolic acid is malleable, less hydrophobic, and rapidly degradable. Due to these characteristics, PLGA can be customized for specific applications.[109] PLGA is one of the most effective biodegradable polymers, known for its controlled and sustained release properties, low toxicity, and biocompatibility with tissues and cells (Table 4).[110] This polymer is soluble in various organic solvents such as acetone, dichloromethane, chloroform, ethyl acetate, and tetrahydrofuran (THF). Due to these characteristics, it can be readily utilized as a carrier for both hydrophobic and hydrophilic drugs.[109]

5. Degradation of Nanofibers

Owing to their high affinity for tissues and blood, nanofiber scaffolds promote wound healing and enhance cell growth. The degradation rate of the nanofibers is a crucial factor in determining the effectiveness of wound healing. Therefore, nanofiber scaffolds should possess a degradation rate suitable for facilitating new tissue regeneration. The degradation rate of these nanofibers varies depending on the material used. Moreover, adjusting the ratio of these materials allows the modulation of the degradation rate.[123,124] The application of these adjustments is discussed below.

Başaran et al. fabricated nanofibers by incorporating heparin-encapsulated PLGA nanoparticles into Sericin/Gelatin (Ser/Gel), as shown in **Figure** 4A–a. To determine the weight loss in the PBS solution for degradation studies, the dry weights of samples with 0/1 Ser/Gel (sericin 0%, gelatin 100%), 1/7 Ser/Gel (sericin 15%, gelatin 85%), and 1/2 Ser/Gel (sericin 35%, gelatin 65%) were measured at each time point (1, 3, and 7 days). As shown in Figure 4A–b, after 7 days, the nanofibers with the highest gelatin content in 0/1 Ser/Gel showed significantly higher weight loss than 1/2 Ser/Gel nanofibers. This indicates that as the gelatin content increases, the degradation rate of the nanofibers increases, which is attributed to the faster degradation rate of gelatin in the biological environment.[125] In another study, Selvaras et al. developed nanofibers of polyurethane (PU), PU/chitosan (PU/CS), PU/chitosan/0.5% elastin (PU/CS/0.5%E), and PU/chitosan/1.0% elastin (PU/CS/1.0%E) (Figure 4B–a). The degradation of these nanofibers was investigated by culturing them in PBS for 60 days and measuring the weight loss at various time intervals. As degradation progressed, the weight loss increased for all nanofibers. In particular, the PU/CS/1.0%E nanofibers exhibited a higher weight loss than the other nanofibers at all time intervals (Figure 4B–b). This suggests that a higher concentration of elastin in the blend promoted the degradation of nanofibers, potentially supporting tissue integration and replacement.[126] Ghorbani et al. blended Zein/PCL in ratios of 70:30, 90:10, and 80:20 to create Zein/PCL

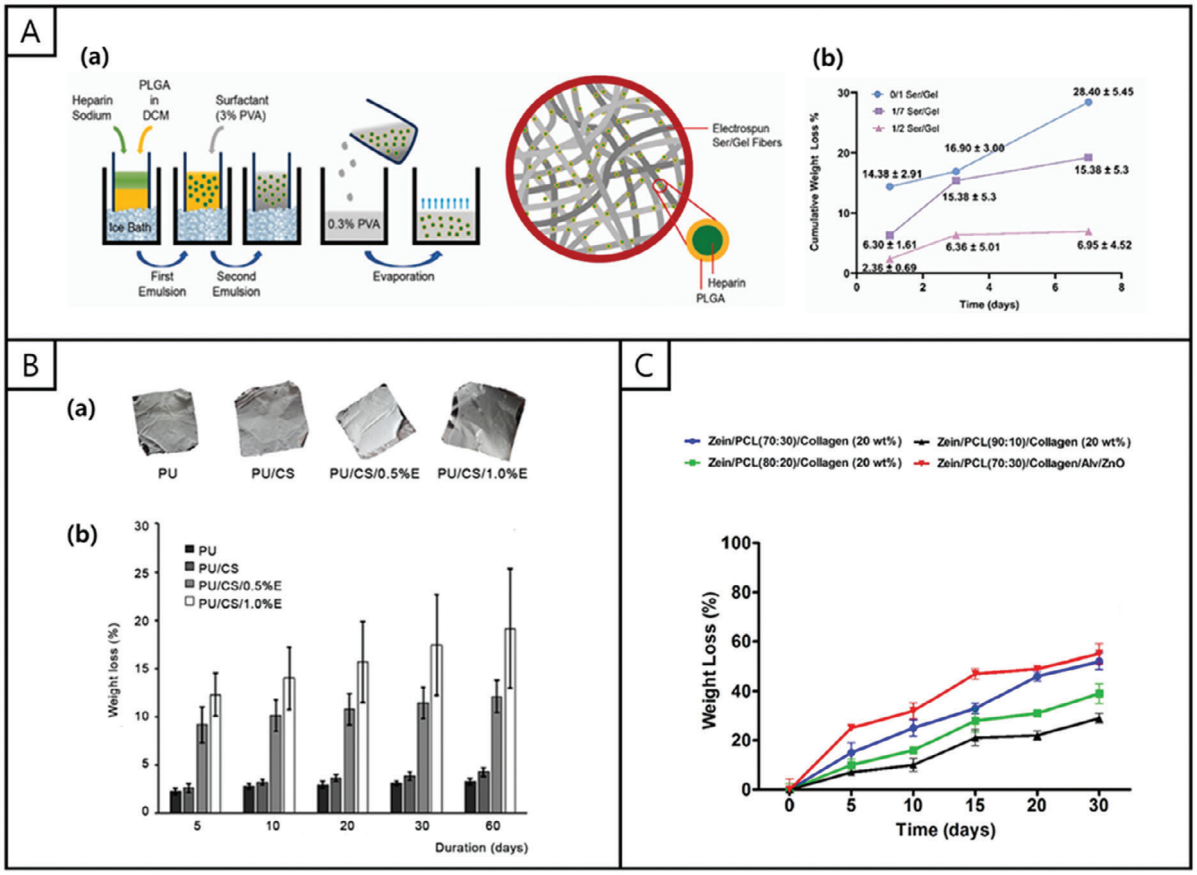

Figure 4. A–a) The schematic representation of the process for preparing nanoparticles of heparin-loaded PLGA and the nanofibers containing PLGA nanoparticles in Ser/Gel. b) Weight loss of 0/1, 1/7, and 1/2 Ser/Gel nanofibers. Reproduced with permission.[125] Copyright 2021, Elsevier B.V. B–a) The appearance of degraded PU, PU/CS, PU/CS/0.5%E, and PU/CS/1%E nanofibers. b) The weight loss measurements for each nanofiber at various time intervals (5, 10, 20, 30, and 60 days). Reproduced with permission.[126] Copyright 2023, Wiley Periodicals LLC. C) The degradation profiles of Zein/PCL (70:30)/Collagen, Zein/PCL (90:10)/Collagen, Zein/PCL (80:20)/Collagen, and Zein/PCL (70:30)/Collagen/Alv/ZnO nanofiber. Reproduced with permission.[127] Copyright 2020, Elsevier B.V.

(70:30)/Collagen, Zein/PCL (90:10)/Collagen, and Zein/PCL (80:20)/Collagen nanofibers. They further developed Zein/PCL (70:30)/Collagen/Aloe-vera (Alv)/Zinc oxide (ZnO) nanofibers by incorporating Alv and ZnO into the Zein/PCL (70:30)/Collagen blend. The degradation profiles of each type of nanofiber were evaluated over time, as shown in Figure 4C. The results showed that Zein/PCL (70:30)/Collagen/Alv/ZnO nanofibers, containing Alv and ZnO nanoparticles exhibited a higher degradation rate than the other fiber types. After 30 days, the nanofibers lost ≈56% of their initial weight. This enhanced degradation can be attributed to the presence of Alv, which reduces the number of intermolecular interactions among collagen molecules and facilitates degradation.[127]

6. Effects of Micro/Nano-Fabrication ECM on Macrophage Polarization

6.1. Classification of Macrophage Polarization

The skin tissue is complex and consists of various cell types. Macrophages are found in various skin tissues.[128] Their types and functions are briefly discussed below and listed in **Table 5**.

Macrophages play a crucial role in regulating the wound-healing process. Their phenotypes evolve with the stage of wound healing.[129] In general, macrophages observed within wounds originate from various sources. They can be classified into two distinct types based on their respective roles in wound healing. Traditionally, they are classified into the classically activated pro-inflammatory M1 phenotype and the alternatively activated anti-inflammatory M2 phenotype. As depicted in **Figure 5B**, it can be observed that during the early stages of wound healing, the macrophages within the wound are mostly of the M1 phenotype, and they transition to the M2 phenotype at ≈5 to 7 days (≈80–85%).[130]

Macrophages play a crucial role in wound healing. Collectively, these functions contribute to the overall healing process by facilitating tissue repair and regeneration. The following roles highlight the importance of macrophages in wound healing:

First, macrophages are responsible for phagocytosis and clearance. They engulf and eliminate bacteria, cellular debris, and dead cells in the wound area, thereby creating a clean environment for healing. Second, macrophages produce enzymes that aid in tissue digestion. These enzymes help break down necrotic tissue, facilitating the removal of damaged or non-viable

Table 5. Macrophage surface markers for skin regeneration.

Macrophage type	Tissue location	Surface main markers	Functions	References
Langerhans cells	Epidermis	CD207, Cd1a, E-cadherin	Presence in the early stages of wound healing, initiation of immune responses, control of inflammation, promotion of upper body closure	[136–138]
Dermal macrophages	Dermis	CD11b, F4/80, CD163, CD64	Responses to pathogens, inflammation and tissue remodeling and maintains tissue homeostasis	[14, 139]
Dermal dendritic cells	Dermis	CD11c, CD1a, CD207, CD209	Antigen presenting cells, accelerated early wound healing, promote angiogenesis, generate ECM components	[140–142]
Subcutaneous macrophages	Dermis (subcutaneous tissue)	CD40, CD206, CD163	Immune control, anti-inflammatory	[143, 144]
Inflammatory Macrophages	Sites of inflammation or tissue damage	CD14, CD163	Transmission of inflammatory cytokines, regulation of inflammation, modulation of the inflammatory microenvironment	[145, 146]
Tissue-resident macrophages	Most tissues in the body	CD64, CD163, F4/80, CD206, CD169	Clearance of dead cell debris, tissue immune surveillance, response to infection and resolution of inflammation, tissue development and remodeling, tissue homeostasis	[147–149]

CD11b, Cd1a, CD11c, CD207, CD209, CD40, CD206, CD163, CD14, CD64, CD169 Cluster of differentiation 11b, 1a, 11c, 207, 209, 40, 206, 163, 14, 64, 169).

tissue from the wound site. Macrophages also promote cell migration, proliferation, and survival. They release various signaling molecules and growth factors that attract and guide other cells involved in wound healing. In addition, macrophages provide a supportive microenvironment that promotes the proliferation and survival of cells necessary for tissue regeneration. Furthermore, macrophages contribute to angiogenesis and the formation of new blood vessels. They attract endothelial cells, which are essential for the development of new blood vessel networks that supply oxygen and nutrients to healing tissues. Macrophages are also involved in the synthesis of ECM components. The ECM provides structural support to cells and aids in tissue organization. Macrophages contribute to ECM synthesis by producing various components, including collagen and FN. Finally, macrophages produce matrix-remodeling enzymes that participate in ECM remodeling. These enzymes help break down and rearrange the ECM, allowing for tissue restructuring and wound closure. Macrophages play diverse critical roles in wound healing. They phagocytose and clear debris, produce enzymes for tissue digestion, promote cell migration and proliferation, facilitate angiogenesis, contribute to ECM synthesis, and produce matrix-remodeling enzymes. Through these functions, macrophages actively contribute to wound healing and facilitate tissue repair and regeneration.[131]

6.1.1. Classically Activated Polarization

In infected tissues, macrophages are initially polarized to the M1 phenotype to aid host defense against pathogens. A key aspect of macrophage polarization is the alteration in the expression of cell surface markers. M1 macrophages overexpress CD80, CD86, and CD16/32 and secrete inflammatory cytokines.[132] During the pro-inflammatory phase of wound healing, M1 macrophages dominate, and exhibit increased phagocytic activity and production of pro-inflammatory cytokines, thereby promoting innate immunity and wound fragmentation. They contribute to wound sterilization and removal of necrotic tissue through their high phagocytic activity. Furthermore, M1 macrophages stimulate the activation of other immune cells in the initial stages of the wound-healing process.[129,130] M1 macrophages are stimulated by Th1 cytokine interferon-gamma (IFN-γ), lipopolysaccharide (LPS), and TNF-α. They secrete IL-12, IL-6, IL-1β, and TNF-α (Figure 5A).[133] LPS promotes the activation of M1 macrophages through Toll-like receptor (TLR) 4. Additionally, IFN-γ plays a role in regulating the expression of macrophage genes encoding cytokine receptors, cell activation markers, and cell adhesion molecules. M1 macrophages play a vital role in host defense against viruses and intracellular bacteria. They generate nitric oxide (NO) and reactive oxygen intermediates (ROI).[134]

6.1.2. Alternatively Activated Polarization

M2 macrophages dominate later in the healing process, are activated by various stimuli, and express growth factors such as VEGF, TGF-β, and IL-10. They help reduce inflammation and promote tissue generation and remodeling. Based on their functional diversity, M2 macrophages can be categorized into the subtypes M2a, M2b, M2c, and M2d, as shown in Figure 5A. These phenotypes represent a continuum of macrophage activities that can change based on cellular characteristics and contextual stimuli rather than being independently segregated. The M2a macrophages induced by IL-4 and IL-13, secrete IL-12, IL-8, IL-10, and other anti-inflammatory cytokines, thereby suppressing inflammation, promoting wound resolution, and facilitating Th2-type immune responses.[130] Furthermore, contributes the ECM formation and supports angiogenesis.[129] M2b macrophages are induced by immune complexes and IL-1β and secrete both pro-inflammatory and anti-inflammatory cytokines

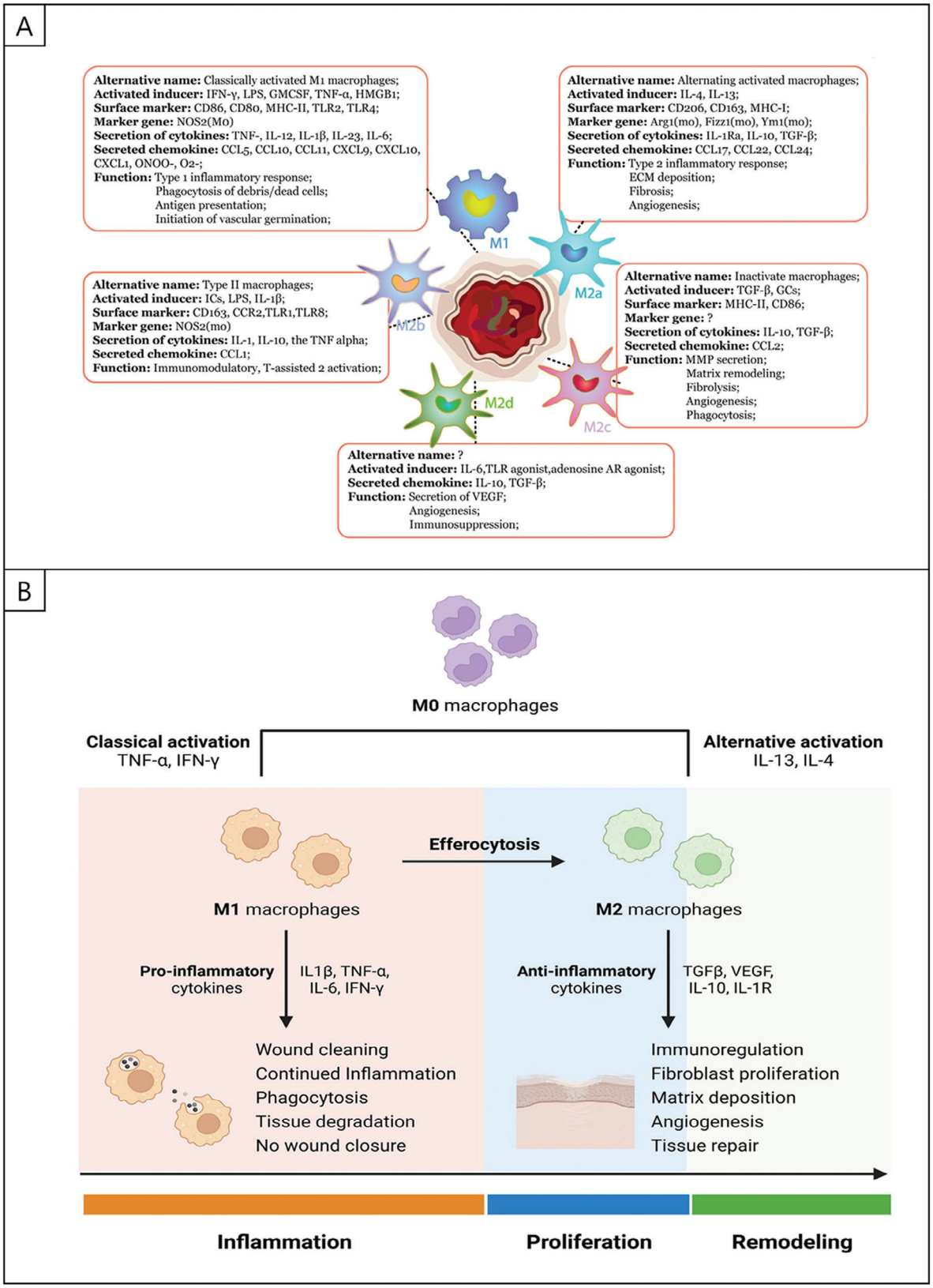

Figure 5. A) Classification of macrophages: M1, M2a, M2b, M2c, M2d, and their functions. Reproduced with permission.[130] Copyright 2021, Wiley-VCH GmbH. B) Polarization of macrophages and their role in the wound healing process. Reproduced with permission.[34] Copyright 2022, Oxford University Press.

Table 6. Topology of nanofibers regulate the macrophage polarization.

	Materials	Polarization	Gene markers	Application	References
Anisotropy	Poly(L-lactide)	M2 phenotype	Arg-1, IL-4, IL-10, TGF-β, iNOS, TNF-α, IL-1β	Facilitated wound healing	[155]
	Fish collagen, poly(lactide-co-glycolide)	M2 phenotype	IL-10, CD68, TGF-β	Promote wound healing	[156]
	Tazarotene, poly(ϵ-caprolactone), hexafluoroisopropanol	M2 phenotype	VEGF-A	Facilitates wound healing by promoting angiogenesis	[157]
Isotropy	Poly(ϵ-caprolactone), hexafluoroisopropanol	M2 phenotype	Arg-1, CD163, CD206, IL-4, TGF-β, iNOS,	Immunomodulatory effects	[158]
	Poly(L-lactide), heparin	General phenotype	CD68	Wound healing effect	[159]
	Polylactic acid, polyethylene glycol, platelet, thymosin β4	M2 phenotype	TNF-α, IL-10, CD206,	Chronic diabetes wound healing	[160]

Arg-1, Arginase-1); IL-4, IL-10, IL-1β, Interleukin-4, 10, 1β); TGF-β, Transforming Growth Factor-β); iNOS, inducible Nitric oxide Synthase); TNF-α, Tumor Necrosis Factor-α); CD68, Cluster of Differentiation 68); VEGF-A, Vascular Endothelial Growth Factor A).

such as IL-6, IL-10, IL-1β, and TNF-α. Based on this cytokine profile, M2b macrophages regulate the magnitude and depth of the immune and inflammatory responses. M2c macrophages, also known as deactivated macrophages, are induced by glucocorticoids and TGF-β. They secrete IL-10, TGF-β, CCL16, and CCL18 and play an important role in processes involving apoptotic cells.[133] M2c macrophages play a role in regulating inflammation during wound healing and in promoting angiogenesis.[130] M2d macrophages are induced by TLR and adenosine A2A receptor agonists and play a role in blood vessel creation.[135]

6.2. Micro/Nanostructures Regulate the Macrophage Polarization

6.2.1. Anisotropy and Isotropy Topology of Nanofibers

Macrophages are highly plastic and can be activated by various stimuli in their microenvironment[150]. It is conventionally believed that the surface chemistry of biomaterials regulates the immune response. However, recent research suggests that the arrangement of the isotropic or anisotropic topology of nanofibers can also influence macrophage polarization (**Table 6**).[130] An anisotropic topology refers to a property that is directionally dependent. This is defined as the difference in the physical characteristics of a specific material measured along different axes. Isotropic topology is a characteristic opposite to anisotropy, indicating a state with no specific direction or preferred orientation.[151]

Several studies have provided insights into this phenomenon. For example, Ren et al. fabricated anisotropic nanofibers using PCL and PEG to understand their effects on macrophage polarization. Immunofluorescence staining was conducted for the M1 phenotype marker iNOS and the M2 phenotype marker Arg-1 to analyze macrophage polarization (**Figure 6A**). The results showed significantly positive staining for iNOS in the PCL group, whereas it was lower in the L-PECL (3% PEG, 9% PCL) and H-PECL (9% PEG, 3% PCL) groups. Arg-1 expression was the highest in the H-PECL group, indicating an opposite trend. This suggests that PCL fibers induce macrophage polarization toward the M1 phenotype while incorporating PEG reduces this shift and promotes polarization toward the anti-inflammatory M2 phenotype.[152] In another study, Huang et al. investigated the effects of anisotropic PLGA and AS (Asiaticoside)/PLGA nanofibers on the phenotype shift of macrophages. As shown in Figure 6B–a, noticeably less stained area was observed for anisotropy AS-PLGA after 2 weeks (with an IOD/area of 14.64 ± 2.282%) and 4 weeks (with an IOD/area of 12.97 ± 1.316%) compared to PLGA, indicating a reduced number of CD86-positive cells, a marker for M1 macrophages. In contrast, the expression of CD163, a surface marker for M2 macrophages, was higher after 2 weeks (with an IOD/area of 6.810 ± 1.528%) and 4 weeks (with an IOD/area of 8.634 ± 1.993%) (Figure 6B—b).[153]

Nakkala et al. fabricated isotropic electrospun PCL/ Dimethyl itaconate (DMI) nanofibers (Figure 6C–a). As shown in Figure 6C–b, the PCL/DMI3.3% and PCL/DMI6.6% nanofibers transplanted into the skin exhibited ≈30% CD86-positive inflammatory cells, which is a marker for M1 macrophages, after 3 days. This ratio further decreased to ≈15% after 7 days. In contrast, the ratio of CD206-positive anti-inflammatory cells, a marker of M2 macrophages, increased from ≈5% on day 3 to 25.1% and 32% on day 7 for the PCL/DMI3.3% and PCL/DMI6.6% nanofibers, respectively. This suggests that isotropically electrospun PCL/DMI nanofibers promote macrophage polarization.[154]

Jia et al. applied macrophages to nanofiber scaffolds after fabricating isotropic and anisotropic P(LLA-CL) nanofibers. As shown in Figure 6D–a, on isotropic nanofibers, macrophages exhibited a typical pancake shape on anisotropic nanofibers, whereas they assumed an elongated form. This observation was consistent with the results of the rhodamine-phalloidin staining. Moreover, the proportions of Arg1 (M2 macrophage marker) and iNOS (M2 macrophage marker) positive macrophages were higher in both the isotropic and anisotropic scaffolds than in the control group

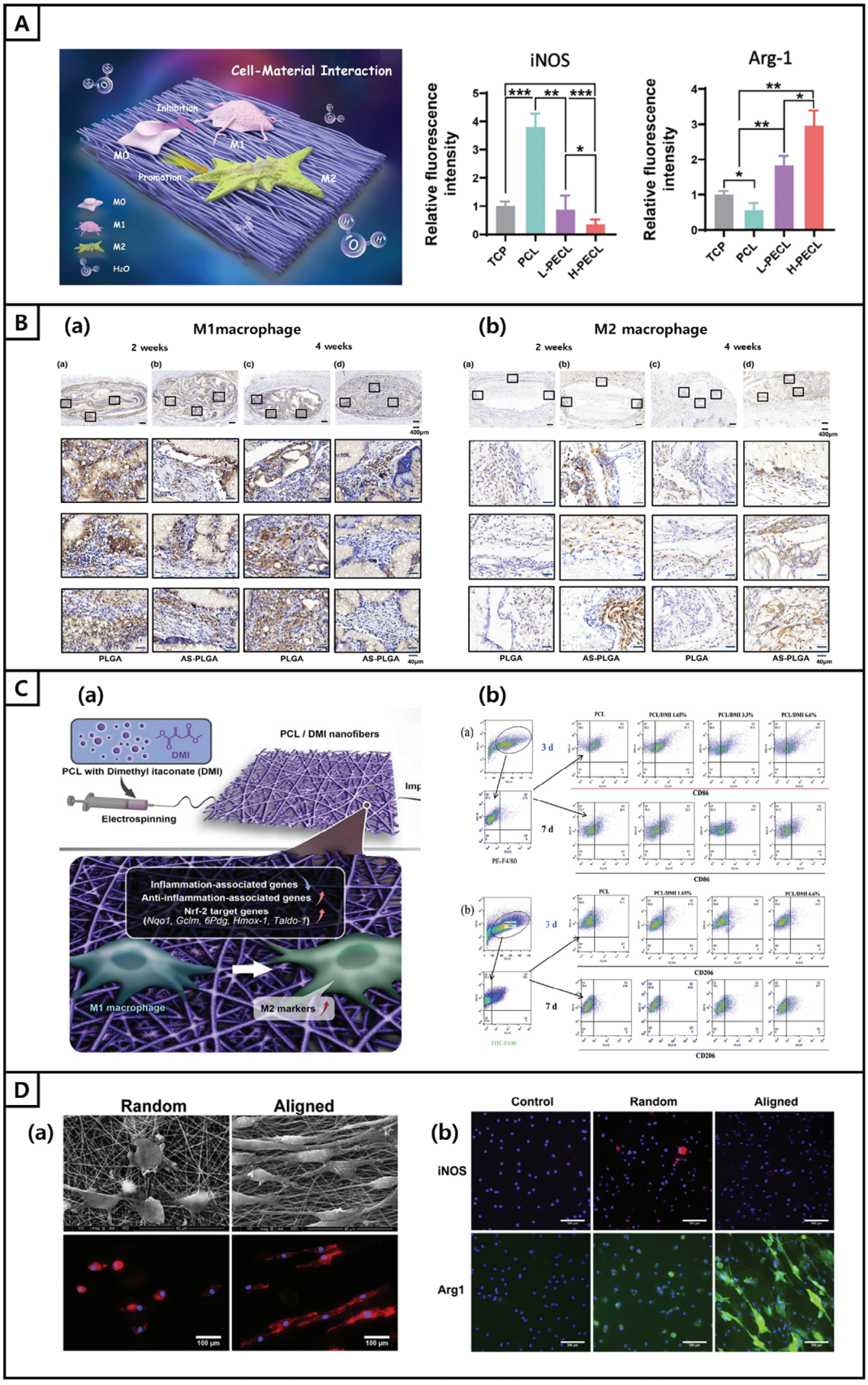

(Figure 6D–b). This suggests that the nanofiber scaffolds activate macrophage polarization.[150]

6.2.2. Effect of Biomaterials on Macrophage Polarization

Micro/nanostructured biomaterials exhibit diverse structural or mechanical features through various structural forms and release cytokines in a spatiotemporal manner, mimicking complex physiological signaling patterns. They can also act as immunomodulators.[130]

M1 macrophages are necessary to achieve complete healing during the initial stages of inflammation. However, if M1 activation becomes excessive or prolonged, it can worsen inflammatory responses and impair tissue regeneration. Therefore, it is important to regulate the transition from the M1 to M2 phenotype, and biomaterials can be utilized for this purpose. Biomaterial-based approaches for macrophage modulation involve modifying the composition, surface properties, and mechanical characteristics of materials. One example is hybrid biomaterials of substances combined with metal ions (e.g., magnesium, zinc, and strontium). Bessa-Gonçalves et al. demonstrated that a scaffold combining fibrinogen, a protein involved in the healing process, with 10 mM magnesium (FgMg10) could regulate inflammation and promote M2 macrophage polarization in vivo.[161]

Liu et al. used co-electrospinning to fabricate PCL and epECM scaffolds. Macrophages within the PCL scaffolds appeared mostly rounded and non-spreading. In contrast, cells within the PCL-epECM/H and PCL-epECM/H-IL-4 scaffolds exhibited an elongated spreading phenotype. Furthermore, the macrophages within the PCL-epECM/H-IL-4 scaffolds exhibited the highest aspect ratio, and their elongation tended to increase over time (**Figure** 7A–a). Macrophage elongation and polarization are closely related. Macrophage elongation plays a role in regulating inflammation and transmitting the signals necessary for tissue regeneration and healing. Immunofluorescence co-staining of CD68 and CD206 revealed that on days 1 and 3, the number of CD206+ cells in the PCL-epECM/H and PCL-epECM/H-IL-4 scaffolds was significantly higher than that in the PCL scaffolds (Figure 7A—b).[162,163] Therefore, this study suggests that hybrid micro/nanofiber scaffolds can provide a favorable microenvironment for tissue regeneration and healing. In another study, Liu et al. dissolved PCL and gelatin in a specific ratio and added magnesium oxide (MgO) at concentrations of 0% and 0.5%. The solution was then electrospuned to obtain nanofibers labeled with PCL/gelatin and MgO-0.5, as shown in Figure 7B. As indicated in the figure, an increase in the markers of M2 macrophages, CD206/CD86, was observed in each group, with particularly high quantitative results in the positive area, especially in MgO-0.5.[164] Niu et al. performed cell diffusion fluorescence microscopy analysis of collagen and HA-collagen nanofibers for 48 h. The results revealed distinct differences in the extent of cell elongation between the collagen and HA-collagen nanofibers. Macrophages on collagen nanofibers exhibited pancake-like morphology, whereas those on HA-collagen nanofibers displayed an elongated shape. SEM images further confirmed this phenomenon. Additionally, the elongation index, determined by dividing the length of the longest axis by the width around the nucleus, was higher for macrophages grown on HA-collagen nanofiber surfaces than those grown on collagen nanofibers (Figure 7C). To evaluate the polarization state of macrophages, the expression of iNOS and Arg-1 was assessed using western blotting. Macrophages cultured on HA-collagen nanofibers exhibited higher levels of Arg-1 than those cultured on collagen nanofibers. Furthermore, pancake-shaped macrophages expressed iNOS, whereas elongated macrophages expressed Arg-1. This suggests a correlation between M2 macrophage polarization and elongated cellular morphology. These findings indicate that macrophages cultured on HA-collagen nanofibers display an elongated morphology, higher expression of Arg-1, and more pronounced M2 polarization than macrophages on collagen nanofibers.[165] Similarly, Taskin et al. categorized samples into five groups: pure gelatin and various ratios of NCO-sP(EO-stat-PO)/gelatin (1:3, 1:2, 1:1, and 2:1). Macrophages cultured on electrospun meshes with different NCO-sP(EO-stat-PO)/gelatin compositions were examined for changes in their differentiation patterns through gene expression analysis. After 7 days of culture, the expression of CD163 and CD206, markers of M2 polarization, increased in all samples except for the 2:1 ratio sample (compared with the reference sample, pure gelatin on day 1; reference line at 1). The pro-inflammatory genes IL-1β and IL-8, markers for M1 polarization, were downregulated after 7 days. The differentiation toward an M2-like phenotype and the decrease in inflammatory markers demonstrate that NCO-sP(EO-stat-PO)/gelatin hydrogel nanofibers can induce immunomodulatory effects on human macrophages.[166]

In another study, Liu et al. produced SF/PLLA nanofibers with mass ratios of 0/100, 20/80, 35/65, and 50/50 and designated them as S/P-0/100-S, S/P-20/80-S, S/P-35/65-S, and S/P-50/50-S, respectively. As shown in Figure 7D–a, the nanofibers exhibited an anisotropic structure. To visualize the inflammatory response to the four types of SF/PLLA nanofibers, immunofluorescent staining of CD68, a marker for macrophages, was performed (Figure 7D–b). The results showed that the expression of CD68 was the highest in S/P-0/100-S. This indicates that the effective polarization of macrophages occurs in S/P-0/100-S.[167]

Yu et al. performed RT-PCR to investigate the effects of porous PLA-based nanofiber membranes on macrophage polarization. Lipopolysaccharide (LPS, 500 ng mL^{-1}), a potent activator of the inflammatory response, was used to induce macrophage polarization toward the pro-inflammatory M1 phenotype. As shown in Figure 7E, after 24 h of co-culture, LPS significantly increased the expression of pro-inflammatory genes (IL-6, IL-1β, TNF-α).

Figure 6. A) Schematic polarization of macrophages cultured in PECL nanofibers and immunofluorescence analysis of iNOS and Arg-1. Reproduced with permission.[152] Copyright 2023, Springer Nature. B) Immunohistochemical analysis of a) M1 and b) M2 macrophage infiltration on PLGA and AS-PLGA nanofiber scaffolds. Reproduced with permission.[153] Copyright 2019, Wiley Periodicals, Inc. C–a) Schematic diagram of PCL nanofibers loaded with DMI. b) Flow cytometry scatter plots of CD86- and CD206-positive cells for subcutaneously implanted PCL, PCL/DMI1.65%, PCL/DMI3.3%, and PCL/DMI6.6% nanofibers on days 3 and 7. Reproduced with permission.[154] Copyright 2021, Wiley-VCH GmbH. D–a) SEM and b) rhodamine-phalloidin staining images of macrophage morphology on isotropy and anisotropy P(LLA-CL) nanofiber membranes. Reproduced with permission.[150] Copyright 2018, Elsevier Ltd.

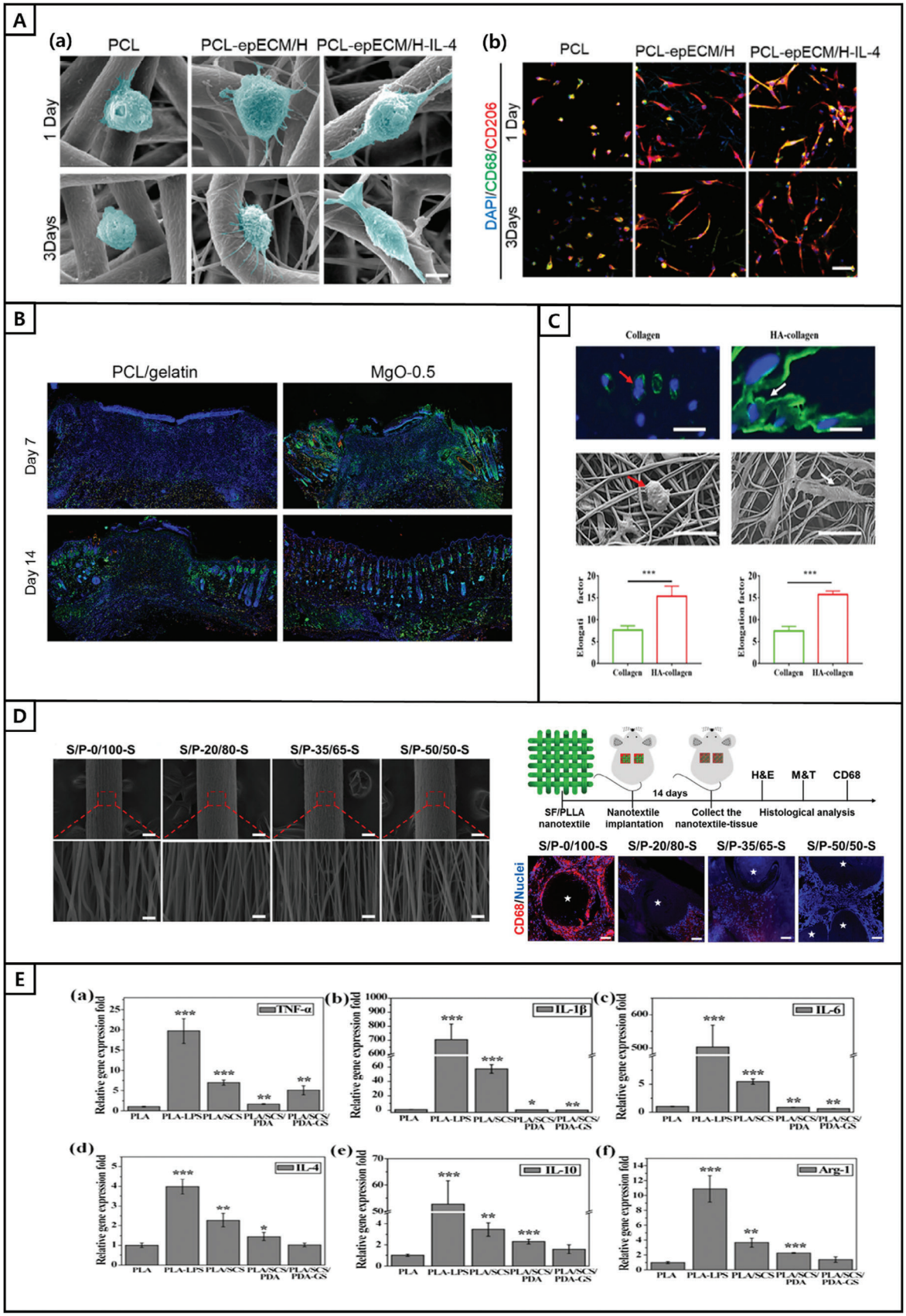

In contrast, the PLA/SCS, PLA/SCS/PDA, and PLA/SCS/PDA-GS groups showed reduced expression of the pro-inflammatory genes. In particular, the PLA/SCS and PLA/SCS/PDA groups exhibited increased expression of anti-inflammatory genes (IL-4, IL-10, and Arg-1).[168] Ryma et al. spontaneously differentiated monocyte-derived macrophages, which were examined for the secretion of cytokines, including IL-6, IL-8, IL-10, IL-1β, TNF- α, and TGF- β1, in the cell culture medium after days 3 and 7. On day 7, there was a significant increase in the release of the M2 marker IL-10 from fibril scaffolds compared with that from fiber scaffolds (POx and PCL) and collagen fibrils. Additionally, on day 3, the macrophages cultured on POx samples exhibited significantly higher IL-10 secretion. TGF-β1, a fibrotic-related M2 marker, showed the lowest release on collagen samples compared with synthetic materials, with no significant differences observed between the 3D and 2D collagen samples. Conversely, TGF-β1 secretion was significantly lower on POx and PCL fibrils than on fiber scaffolds. Moreover, the release of M1 markers TNF-α, IL-6, IL-8, and IL-1β was minimal on fiber scaffolds, exhibiting a decline or consistently low levels throughout the culture period. In contrast, on fibril scaffolds, the secretion of IL-1β and TNF-α started at elevated levels on day 3 and exhibited a substantial decline over time.[169]

7. Application in Skin Tissue Regeneration

Macrophages can polarize into classically activated M1 and alternately activated M2 macrophages, making them capable of treating damaged skin tissue. In addition, electrospun micro/nanofibers produced using natural and synthetic materials can serve as scaffolds with ECM-like structures that support skin regeneration and tissue formation. The applications of these innovative technologies and materials for skin tissue regeneration are discussed below and given in **Table 7**.

Gao et al. fabricated PLGA nanofibers using electrospinning and coated them with membranes derived from LPS and IFN-γ activated macrophages (RCM). Subsequently, RCM-fiber-BMMSCs loaded with bone marrow-derived MSCs (BMMSCs) were prepared (**Figure** 8A–a), and the effects of these compounds on wound healing in diabetic rats were investigated. As shown in Figure 8A–b, the group treated with RCM-fiber-BMMSCs exhibited a drastic increase in wound closure compared with the other four groups from day 5 onwards. Additionally, the skin regenerated by RCM-fiber-BMMSCs demonstrated a mature epithelial structure with less thinning of the epidermis, confirming the rapid regeneration effect of the epidermal skin. Moreover, the anti-inflammatory effects were also investigated. The proportion of F4/80+CD86+ and F4/80+TNF-α+ macrophages in the wound area was minimized with RCM-fiber-BMMSCs treatment. In contrast, the proportion of F4/80+CD206+ macrophages was the highest after 7 days of treatment. This indicates that RCM-fiber-BMMSCs contribute to reducing inflammation in wounds.[170] Also, Zhang et al. investigated the therapeutic effects of a silk fibroin/gelatin (SF/GT) nanofiber dressing loaded with astragaloside IV (AS) on acute wounds. Rats with deep epidermal injuries on their dorsal surfaces were treated with saline, blank nanofiber dressing (blank control), AS solution, or AS-loaded SF/GT nanofiber dressing. The results showed that wounds treated with the AS-loaded SF/GT nanofiber dressing exhibited significantly higher wound closure rates than the control groups at 3, 6, and 9 days post-treatment. Additionally, VEGF content and the number of macrophages in the wound area significantly increased 7 days post-treatment compared with the control groups. Scanning electron microscopy and histological analyses confirmed the enhanced scar inhibition effect. This suggests that the AS-loaded SF/GT nanofiber dressing effectively promotes wound healing and has scar-inhibiting effects, making it a promising therapeutic agent for treating acute wounds.[171]

In another study, He et al. developed a PCL/Quaternized chitosan-graft-polyaniline (QCSP) nanofiber wound dressing that promoted wound healing. As shown in Figure 8B–a, Tegaderm film and the PCL/QCSP0 and PCL/QCSP15 groups exhibited low TNF-α expression throughout the entire wound healing period, indicating that QCS and polyaniline endowed antimicrobial abilities to the wound dressing to reduce inflammation. Additionally, PCL/QCSP15 showed significantly higher VEGF expression than Tegaderm. This suggests that PCL/QCSP15 accelerates wound healing more than Tegaderm film. Additionally, the antibacterial activity of the PCL/QCSP nanofiber wound dressing was evaluated. The results showed excellent killing ratios (> 90%) against both *S. aureus* and *Escherichia coli* for all PCL/QCSP groups except for PCL/QCSP0 (Figure 8B–b). This implies that PCL/QCSP nanofiber wound dressings possess antibacterial properties, reduce bacterial load, and decrease inflammation in the wound, ultimately enhancing the rate of wound healing.[172] As well, Wu et al. developed an ECM-like gelatin nanofiber matrix to modulate macrophages and induce anti-inflammatory effects. After 4 h of macrophage culture, the number of macrophages on the nanofiber matrix (634 ± 40 cells mm^{-2}) was twice as high as that on the film (240 ± 25 cells mm^{-2}). Furthermore, after 24 h of culture, the number of macrophages on the nanofiber matrix (1240 ± 98 cells mm^{-2}) was significantly higher than that on the film (760 ± 112 cells mm^{-2}). Moreover, ≈80% of the macrophages maintained a round morphology on the nanofiber matrix, whereas this proportion was ≈50% on the film. Additionally, some macrophages spread out in a flat shape on the film. Many macrophages can activate inflammatory responses and promote the processes necessary for wound healing. In addition, the round morphology of the macrophages facilitates film interactions with other cells, aiding tissue regeneration and

Figure 7. Effect of micro/nano biomaterials fibers in macrophage polarization. A–a) SEM showing the morphology of macrophages cultured on different scaffolds on days 1 and 3. b) The number of CD206+ cells in each respective scaffold. Reproduced with permission.[162] Copyright 2022, Elsevier B.V. B) Representative immunofluorescence images of wound tissue sections stained with CD206/CD86 on days 7 and 14. Reproduced with permission.[164] Copyright 2022, Wiley Periodicals LLC. C) The shape of macrophages in Collagen and HA-collagen nanofibers. Reproduced with permission.[165] Copyright 2021, Springer Nature. D–a) Experimental design schematic. b) CD68 (red) immunofluorescence staining images of 0/100-S, S/P-20/80-S, S/P-35/65-S, and S/P-50/50-S nanofibers. Reproduced with permission.[167] Copyright 2022, Elsevier Ltd. E) The relative gene expression fold of Raw 264.7 cells in each group after 24 h. Reproduced with permission.[168] Copyright 2023, Springer Nature.

Table 7. Properties of nanofibers applied to skin tissue regeneration.

Nanofibers	Size [nm]	Properties	Cell line	Application	References
Graphene nanosheet-chitosan/gelatin (0.15% GNS)	106 ± 30	Porosities (0.15% GNS): 90%	Normal human fibroblast	Normal human fibroblasts cell: Uniform distribution, more intense formation, Percent of in vitro wound closure: 97% (after 48 h)	[179]
PU/EEP-PCL/Gelatin	237.3 ± 65.1	Elongation at maximum load 45.9 ± 3.3%, tensile strength 1.7 ± 0.9 MPa	L929 fibroblast	Area percentage of the wound area (days 1, 5, 10, and 15 respectively): 98.2%, 42.1%, 25.4%, and 8.5%	[180]
Chitosan/poly (ethylene oxide)/collagen/curcumin	75 ± 0.91	Young's modulus 6151 ± 270 Pa	Human dermal fibroblast (HDF)	Average wound area (days 5, 10, 15, and 20 respectively): 36% ± 18%, 73% ± 11%, 91% ± 4.5%, 97% ± 0.9%	[181]
Poly (3- hydroxybutyric acid)/ gelatin- coccinia grandis leaf extract-collagen	240 ± 30 (average)	Young's modulus [MPa] 2.99 ± 0.16	NIH 3T3 fibroblast, HaCaT keratinocytes	NIH 3T3 fibroblast, HaCaT keratinocytes: Significant increase in cell survive (after 7 days)	[182]
Chitosan-gelatin/ hyaluronic acid	217.5 ± 40.7	Tensile strength / Young's modulus [MPa] 9.11 ± 0.94 / 208 ± 20	Human dermal fibroblasts (HDF)	HDF cell: Significantly higher proliferation rates (during the first 24 h), wound (14 days after treatment): Almost sutured	[183]
PEU4:6(PCL:dECM(%) = 40:60)	72.18 ± 5.47	Tensile strength [MPa], elongations [mm/mm] 3.7 ± 0.2 / 0.6 ± 0.1	Human dermal fibroblast (HDF), HaCaT keratinocytes	Wound area (days 7, 14, 21 respectively): 42.1% ± 13.8%, 7.2% ± 3.4%, 1.3% ± 1.0%	[184]
Hyaluronic acid-silk fibroin/Zinc oxide (3 wt%)	178 ± 17	Tensile modulus [MPa] / breaking strain [%] 7.12 ± 0.17 / 40.12 ± 0.18	HaCat keratinocytes	Wound closure (days 0 and 7 respectively): 33.13 ± 2.31%, 55.02 ± 1.35%	[185]
Catechol-functionalized hyaluronic acid/gelatin	≈450 to 550	Tensile strength [kPa] 46.1 ± 16.3	NIH/3T3 fibroblasts	NIH/3T3 fibroblasts: adhesion to the matrix surface of nanofiber, Wound area: 35% decreased (for 7 days)	[186]

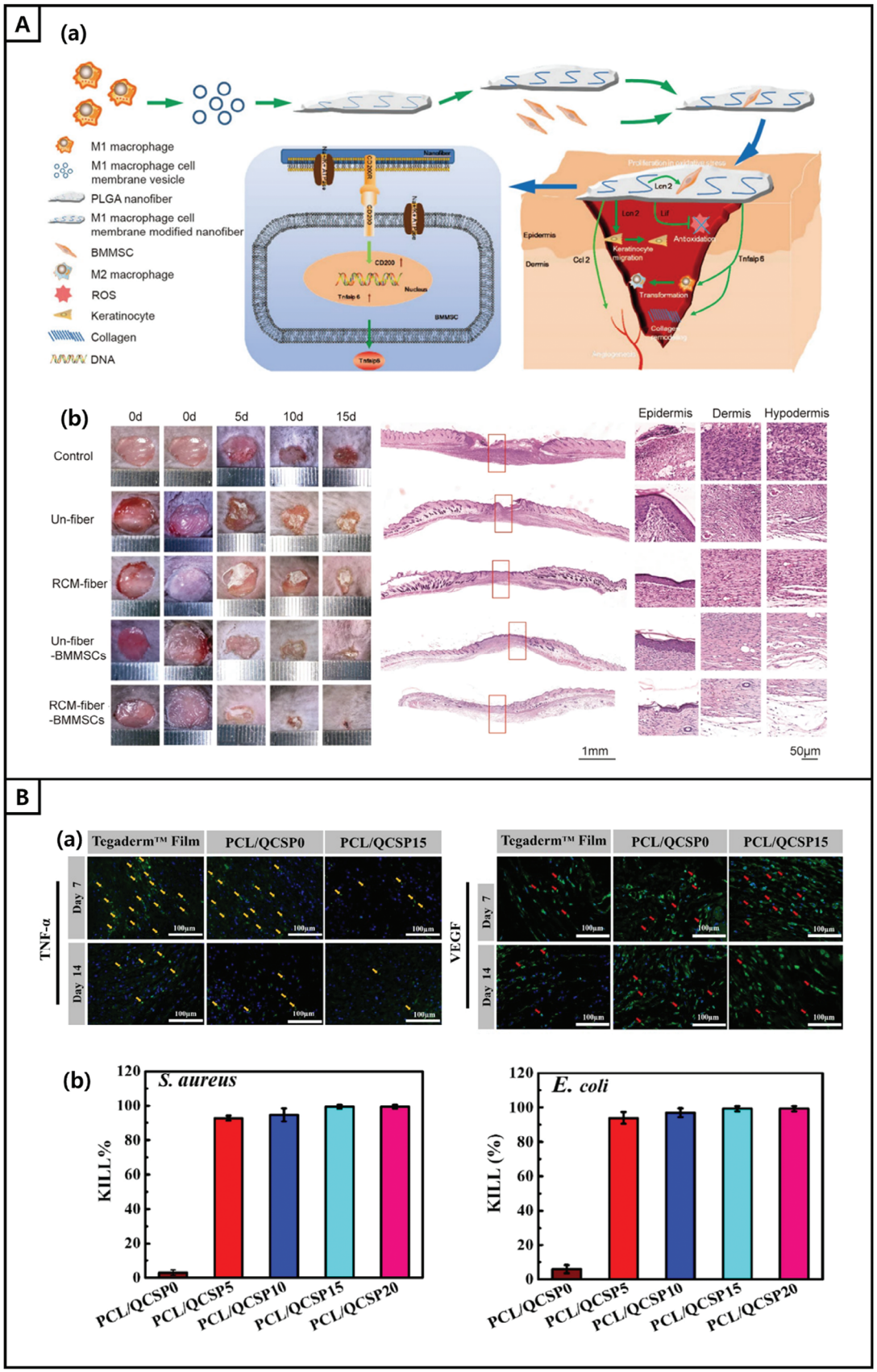

healing. In this regard, a nanofiber matrix is considered more effective than a film for wound healing.[173]

Chen et al. designed electrospun fibers coated with inner–outer IL-10 to programmably activate sequential immune responses during wound healing. They constructed electrospun PLA fibers without IL-10 loading (PF), electrospun fibers loaded with IL-10 internally, and electrospun fibers loaded with IL-10 externally to investigate the release characteristics of IL-10-loaded electrospun fibers (**Figure** 9A–a). After seeding fibroblast cells onto the electrospun meshes of the PF, In-IL-10@PF, PF@Ex-IL-10, and PF-IL-10 groups, all four groups showed strong attachment and significant proliferation of fibroblasts on the fiber surfaces after 3 days (Figure 9A–b). This indicates excellent biological compatibility for all four groups. To evaluate the biological effects on macrophages (Figure 9A–c), macrophages stimulated with PF and PF-IL-10, with high expression of CD163 and CD206, were polarized into M2 macrophages. Additionally, the TGF-β1 concentration in the PF-IL-10 group reached 3.6 times that of the control group. This suggests that PF-IL-10 can suppress inflammation and contribute to scarless wound healing.[174] Similarly, Zhong et al. developed RA-BSP-PVA@PLA nanofibers, where RA represented rosmarinic acid, BSP represented Bletilla striata polysaccharide, PVA represented polyvinyl alcohol, and PLA represented polylactic acid. To demonstrate the wound healing effects, the wound closure rates were measured on days 5, 10, and 15 of treatment. As shown in Figure 9B, RA-BSP-PVA@PLA nanofibers reduced wound size compared with the other groups on days 5 and 10 of treatment, indicating the potential of RA-BSP-PVA@PLA as a wound dressing material. Furthermore, on the 5th day after RA-BSP-PVA@PLA treatment, the expression of CD206, a marker for M2 macrophages, reached the maximum among the four groups. In contrast, the control group achieved high levels of CD86 and minimal levels of CD206 even on the 10th day, preventing the transition to subsequent healing stages. This suggests that RA-BSP-PVA@PLA promotes wound healing.[175]

Sheikholeslam et al. characterized an elastic scaffold that could promote skin regeneration by developing a novel tissue engineering support material. In this study, a gelatin-based electrospun polyurethane (PU)-Gelatin scaffold was prepared using biodegradable PU. F4/80 staining for immune fluorescence imaging revealed a significant presence of macrophages in the wound area on the Gel80—PU20 scaffold. Furthermore, using CD206 as a marker for M2-type macrophages in the stained sections demonstrated that macrophages were present within the scaffold. Moreover, in vivo, the Gel80-PU20 scaffold underwent degradation in the wound environment and allowed deeper cell infiltration when applied to mouse wounds. This demonstrated the potential of electrospun Gel80-PU20 scaffolds to generate tissue substitutes and overcome the limitations of existing wound healing matrices.[176] Zhou et al. developed chitosan (CS)/PCL nanofibers containing zinc ions (Zn). To evaluate the antibacterial performance of the nanofibers, the shake flask method was employed using *E. coli* and *S. aureus*. The results showed that CS/PCL nanofibers without zinc ions exhibited antibacterial rates of 30.8 ± 2.1% for *E. coli* and 30.2 ± 1.4% for *S. aureus*, whereas CS-Zn/PCL nanofibers with zinc ions showed excellent antibacterial rates of 90.0 ± 1.5% and 87.5 ± 4.2% for *E. coli* and *S. aureus*, respectively. These findings indicate that the CS-Zn/PCL nanofibers possess outstanding antibacterial activity, protecting against microbial infections and promoting wound healing. Furthermore, the expression of representative inflammatory factors, IL-6 and TNF-α, was detected using ELISA kits. The results revealed that the CS-Zn/PCL nanofibers significantly inhibited the expression of these factors compared to CS/PCL nanofibers. Additionally, the CS-Zn/PCL nanofibers exhibited high levels of CD206 expression, suggesting that zinc ions may regulate the polarization of pro-inflammatory (M1) macrophages to immunomodulatory (M2) macrophages, thereby modulating inflammatory responses. Based on these results, it can be inferred that the CS-Zn/PCL nanofibers promote wound healing.[177]

Zhang et al. also utilized chitosan in employing an electrospinning strategy to develop CS-PVA-ANE (Pulsatilla, anemoside B4) nanofiber dressings. The reduction in blood loss may accelerate wound healing by promoting blood clotting. Results from assessing blood loss in mice 60 s after injury revealed a significant decrease of 32.7 mg in the sample I (CS-PVA) group, and all sample II (CS-PVA-0.1 ANE), sample III (CS-PVA-0.2 ANE), sample IV (CS-PVA-0.3 ANE), and sample V (CS-PVA-0.4 ANE) groups exhibited lower blood loss compared with the control group. This hemostatic property arises from chitosan-induced red blood cell and platelet aggregation (Figure 9C–a). Additionally, flow cytometry analysis showed that 19.8% of M0 macrophages differentiated into the M1 phenotype, and after pretreatment with the CS-PVA-ANE supernatant, 64.6% differentiated into the M2 phenotype (Figure 9C–b). This indicates that the CS-PVA-ANE nanofibers effectively convert macrophages from the M1 to the M2 phenotype, demonstrating potent anti-inflammatory properties.[178]

8. Conclusion and Future Perspective

This review provides information on micro/nanofibers with ECM-mimicking anisotropic and isotropic topologies for skin tissue regeneration and the modulation of macrophage polarization. Electrospun fibers have been shown to effectively regulate the expression of essential cytokines, growth factors, and ECM components that are crucial for tissue repair. Moreover, owing to their excellent physical and biological properties, they are considered promising materials for wound healing compared with conventional wound dressings. Micro/nanofibers, obtained by incorporating ECM components and bioactive molecules to mimic the structure and composition of the ECM, possess a structure similar to that of the skin tissue, thereby promoting ECM generation and serving as an excellent scaffold for skin tissue regeneration. This structural similarity enhances the attachment and growth of macrophages. Furthermore, fibers with anisotropic

Figure 8. A–a) Schematic diagram of the fabrication process of RCM-fiber-BMMSC nanofibers. b) Images of wounds on days 0, 5, 10, and 15 in each group and representative images of H&E staining on day 15 of each group's day 15 wound (scale bar = 1 mm), high-resolution images of the epidermis, dermis, and subcutaneous tissue (scale bar = 50 μm). Reproduced with permission.[170] Copyright 2022, Springer Nature. B–a) Immunofluorescence staining markers with TNF-α (green) and VEGF (green) of wound tissue regenerated on days 7 and 14. b) Antibacterial activity for *S. aureus* and *E. coli* of PCL/PCSP nanofibers. Reproduced with permission.[172] Copyright 2019, Elsevier B.V.

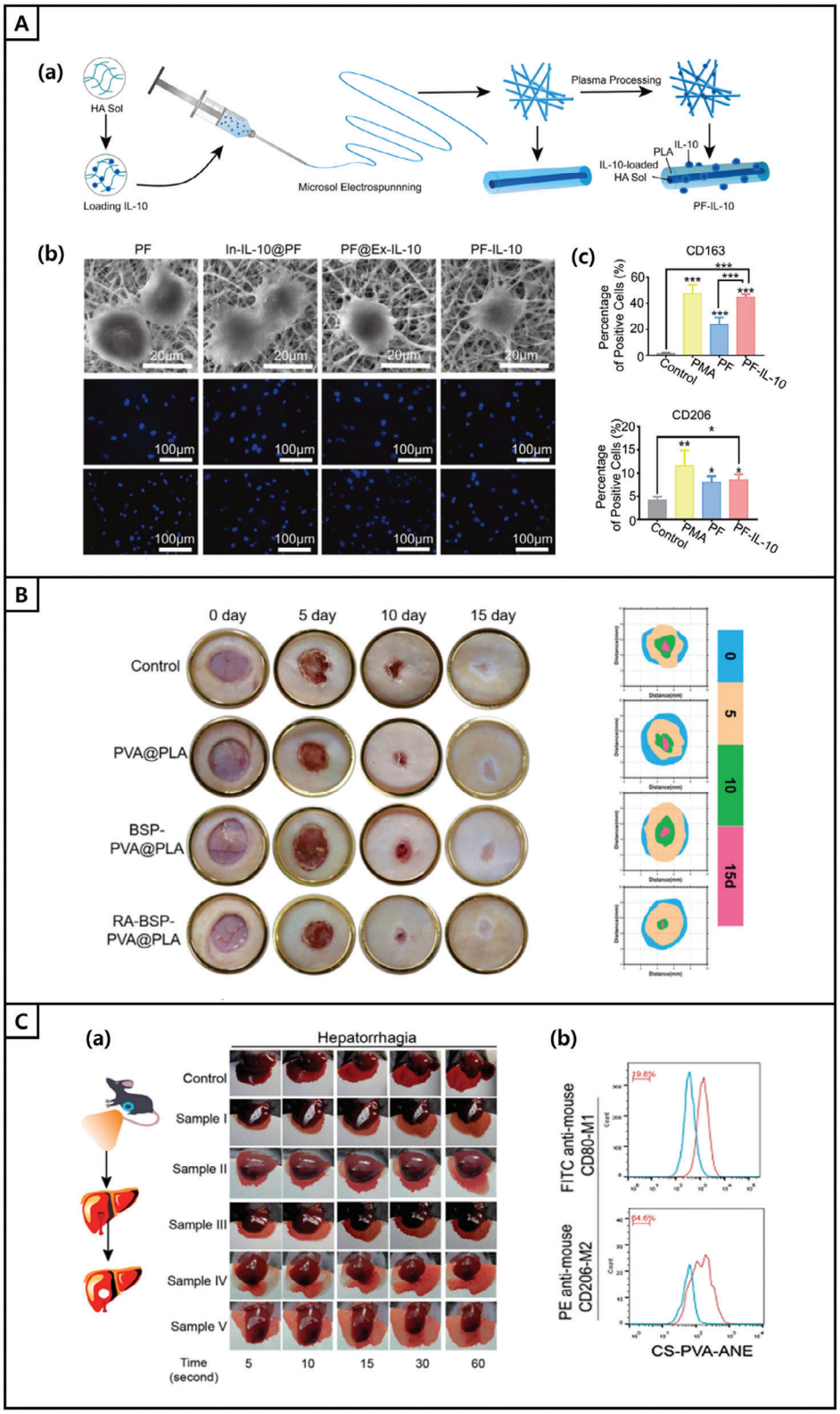

Figure 9. A–a) Electrospinning nanofibers schematic with inner-outer IL-10. b) SEM images of fibroblast cells in each group and nuclear fluorescence staining of live cells on days 1 and 3. c) Statistical analysis of CD163 and CD206 expression. Reproduced with permission.[174] Copyright 2021, Elsevier B.V. B) Mouse wound healing photo of control, PVA@PLA, BSP-PVA@PLA, and RA-BSP-PVA@PLA. Reproduced with permission.[175] Copyright 2023, Elsevier B.V. C–a) Hemostatic characteristics of each sample. b) Macrophage flow cytometry patterns stained with CD80 and CD206 of CS-PVA-ANE. Reproduced with permission.[178] Copyright 2024, Taylor & Francis.

and isotropic topologies have shown promising results in attenuating M1 macrophage polarization, suppressing inflammation, and regulating M2 macrophage polarization. These polarization changes are crucial in promoting wound healing and tissue regeneration. Furthermore, these ECM-mimicking micro/nanofibers exhibit high biocompatibility, allowing them to suppress immune and inflammatory responses while minimizing the risk of infection.

Because of these advantages, micro/nanofibers with ECM-mimicking anisotropic and isotropic topologies have gained significant attention in skin tissue regeneration and have great potential for further advancement. However, further research is required to enhance skin regeneration and modulate macrophage polarization. First, developing more efficient delivery systems for bioactive molecules enhances the biological functionality of fibers. Second, the control of mechanical strength, elasticity, surface properties, and other characteristics of the fibers provides an environment that closely resembles the native ECM and skin tissue, thereby improving the regenerative capacity of the fibers. The third is the advancement of manufacturing techniques for mass production and the exploration of more cost-effective approaches. Finally, investigation of long-term effects and stability to provide reliable data for clinical applications. Through continued research in these areas, it will be possible to develop advanced nanofibers that can effectively promote skin tissue regeneration. Further research and development in this field can potentially contribute to more effective strategies for macrophage-activated wound healing and skin regeneration by altering micro/nanofiber properties and morphologies.

Acknowledgements

H.P. and T.V.P. contributed equally to this work. This study was supported by the "Basic Science Research Program" through the "National Research Foundation of Korea" funded by the "Ministry of Education" (NRF- 2018R1A16A1A03025582, NRF-2019R1D1A3A03103828, and NRF2022R1I1A3063302). This research was supported by the MSIT (Ministry of Science and ICT), Korea, under the Innovative Human Resource Development for Local Intellectualization support program (IITP-2023-RS-2023-00260267*) supervised by the IITP "(Institute for Information & communications Technology Planning & Evaluation)"

Conflict of Interest

The authors declare no conflict of interest.

Keywords

anisotropy and isotropy topology, extracellular matrix-inspired micro/nanofibers, electrospinning, macrophage polarization, skin tissue regeneration

Received: November 22, 2023
Revised: January 16, 2024
Published online:

[1] S. Suganya, J. Venugopal, S. Ramakrishna, B. S. Lakshmi, V. R. G Dev, *Int. J. Biol. Macromol.* **2014**, *68*, 135.
[2] S. A. Eming, P. Martin, M. Tomic-Canic, *Sci. Transl. Med.* **2014**, *6*, 265sr6.
[3] Y. D. Nokoorani, A. Shamloo, M. Bahadoran, H. Moravvej, *Sci. Rep.* **2021**, *11*, 16164.
[4] B. P. Chan, K. W. Leong, *Eur. Spine J.* **2008**, *17*, 467.
[5] I. Negut, G. Dorcioman, V. Grumezescu, *Polymers* **2020**, *12*, 2010.
[6] A. Salerno, P. A. Netti, *J. Funct. Biomater.* **2023**, *14*, 101.
[7] R. Hama, J. W. Reinhardt, A. Ulziibayar, T. Watanabe, J. Kelly, T. Shinoka, *Biomimetics* **2023**, *8*, 130.
[8] A. Hernández-Rangel, E. S. Martin-Martinez, *J. Biomed. Mater. Res., Part A* **2021**, *109*, 1751.
[9] A. Hasan, M. Morshed, A. Memic, S. Hassan, T. Webster, H. Marei, *Int. J. Nanomed.* **2018**, *13*, 5637.
[10] V. Harish, D. Tewari, M. Gaur, A. Bihari Yadav, S. Swaroop, M. Bechelany, A. Barhoum, *Nanomaterials* **2022**, *12*, 457.
[11] S. L. Sim, S. Kumari, S. Kaur, K. Khosrotehrani, *Biomolecules* **2022**, *12*, 1659.
[12] A. Hassanshahi, M. Moradzad, S. Ghalamkari, M. Fadaei, A. J. Cowin, M. Hassanshahi, **2022**, *11*, 2953.
[13] S. Y. Kim, M. G. Nair, *Immunol. Cell Biol.* **2019**, *97*, 258.
[14] D. A. Yanez, R. K. Lacher, A. Vidyarthi, O. R. Colegio, *Pfluegers Arch.* **2017**, *469*, 455.
[15] T. J. Koh, L. A. DiPietro, *Expert Rev. Mol. Med.* **2011**, *13*, 23.
[16] T. A. Wynn, K. M. Vannella, *Immunity* **2016**, *44*, 450.
[17] A. Gomez, K. Z. Sabin, K. Echeverri, *Dev. Dyn.* **2020**, *249*, 834.
[18] T. K. Rajab, T. J. O'Malley, V. Tchantchaleishvili, *Artif. Organs* **2020**, *44*, 1031.
[19] D. L. Kusindarta, H. Wihadmadyatami, in *Tissue Regeneration* (Ed: H. A. hay El-Sayed Kaoud), IntechOpen, London **2018**.
[20] N. K. Karamanos, A. D. Theocharis, Z. Piperigkou, D. Manou, A. Passi, S. S. Skandalis, D. H. Vynios, V. Orian-Rousseau, S. Ricard-Blum, C. E. H. Schmelzer, L. Duca, M. Durbeej, N. A. Afratis, L. Troeberg, M. Franchi, V. Masola, M. Onisto, *FEBS J.* **2021**, *288*, 6850.
[21] D. J. Vaca, A. Thibau, M. Schütz, P. Kraiczy, L. Happonen, J. Malmström, V. A. J. Kempf, *Med. Microbiol. Immunol.* **2020**, *209*, 277.
[22] Y. Huang, T. R. Kyriakides, *Matrix Biol. Plus* **2020**, *6*, 100037.
[23] G. Cloutier, A. Sallenbach-Morrissette, J.-F. Beaulieu, *Tissue Cell* **2019**, *56*, 71.
[24] S. Younesi, H. Parsian, *Turk. J. Gastroenterol.* **2019**, *30*, 524.
[25] A. Bennasroune, B. Romier-Crouzet, S. Blaise, M. Laffargue, R. G. Efremov, L. Martiny, P. Maurice, L. Duca, *Matrix Biol.* **2019**, *84*, 57.
[26] K. Wang, X. Meng, Z. Guo, *Front. Cell Dev. Biol.* **2021**, *9*, 2956.
[27] N. Levi, N. Papismadov, L. Solomonov, I. Sagi, V. Krishanovsky, *FEBS J.* **2020**, *287*, 2636.
[28] C. Bertsch, H. Maréchal, V. Gribova, B. Lévy, C. Debry, P. Lavalle, L. Fath, *Adv. Healthcare Mater.* **2023**, *12*, 2203115.
[29] J. Patten, K. Wang, *Adv. Drug Delivery Rev.* **2021**, *170*, 353.
[30] N. Mohammadzadeh, I. G. Lunde, K. Andenæs, M. E. Strand, J. M. Aronsen, B. Skrbic, H. S. Marstein, C. Bandlien, S. Nygård, J. Gorham, I. Sjaastad, S. Chakravarti, G. Christensen, K. V. T. Engebretsen, T. Tønnessen, *Sci. Rep.* **2019**, *9*, 9206.
[31] R. Martinez, S. Peralta Galisteo, H. Castán, M. E. Morales Hernández, *Int. J. Cosmet. Sci.* **2020**, *42*, 529.
[32] B. S. Park, J. Lee, J. H. Jun, *Clin. Exp. Reprod. Med.* **2021**, *48*, 303.
[33] M. J. V. White, P. S. Briquez, D. A. V. White, J. A. Hubbell, *NPJ Regener. Med.* **2021**, *6*, 76.
[34] A. B. Sousa, A. P. Águas, M. A. Barbosa, J. N. Barbosa, *Regener. Biomater.* **2022**, *9*, rbac065.
[35] S.-M. Karppinen, R. Heljasvaara, D. Gullberg, K. Tasanen, T. Pihlajaniemi, *F1000Research*, **2019**, *8*.
[36] R. B. Diller, A. J. Tabor, *Biomimetics* **2022**, *7*, 87.
[37] Y. Yang, Y. Du, J. Zhang, H. Zhang, B. Guo, *Adv. Fiber Mater.* **2022**, *4*, 1027.

[38] V. A. S. David, V. R. Güiza-Argüello, M. L. Arango-Rodríguez, C. L. Sossa, S. M. Becerra-Bayona, *Front. Bioeng. Biotechnol.* **2022**, *10*, 194.
[39] N. Fine, N. Tasevski, C. A. McCulloch, H. C. Tenenbaum, M. Glogauer, *Front. Immunol.* **2020**, *11*, 571085.
[40] M. Rodrigues, G. C. Gurtner, *Curr. Pathobiol. Rep.* **2017**, *5*, 333.
[41] H. N. Wilkinson, M. J. Hardman, *Open Biol.* **2020**, *10*, 200223.
[42] R. Peng, S. Zhang, Y. Yao, J. Wang, X. Zhu, R. Jiang, J. Zhang, W. Zhang, C. Wang, *Chem. Eng. J.* **2023**, *453*, 139669.
[43] T. M. Subrahmanya, A. B. Arshad, P. T. Lin, J. Widakdo, H. K. Makari, H. F. M. Austria, C.-C. Hu, J.-Y. Lai, W.-S. Hung, *RSC Adv.* **2021**, *11*, 9638.
[44] X. Liu, H. Xu, M. Zhang, D.-G. Yu, *Membranes* **2021**, *11*, 770.
[45] B. Azimi, H. Maleki, L. Zavagna, J. G. De la Ossa, S. Linari, A. Lazzeri, S. Danti, *J. Funct. Biomater.* **2020**, *11*, 67.
[46] Y. Xu, G. Shi, J. Tang, R. Cheng, X. Shen, Y. Gu, L. Wu, K. Xi, Y. Zhao, W. Cui, L. Chen, *Sci. Adv.* **2020**, *6*, abc2036.
[47] J. Li, S. Zhang, C. He, J. Ling, *Int. J. Biol. Macromol.* **2024**, *254*, 127685.
[48] C. Cui, S. Sun, X. Li, S. Chen, S. Wu, F. Zhou, J. Ma, *Int. J. Biol. Macromol.* **2022**, *205*, 500.
[49] S. Sun, C. Ding, X. Liu, Y. Zhao, J. Zhang, Q. Ding, Y. Zhang, Y. Zhang, M. Hao, Y. Zheng, W. Liu, M. Yang, *Biomater. Adv.* **2022**, *135*, 212734.
[50] Y. Yue, X. Gong, W. Jiao, Y. Li, X. Yin, Y. Si, J. Yu, B. Ding, *J. Colloid Interface Sci.* **2021**, *592*, 310.
[51] A. Haider, S. Haider, I.-K. Kang, *Arabian J. Chem.* **2018**, *11*, 1165.
[52] A. R. Unnithan, R. Arathyram, C. S. Kim, in *Nanotechnology Applications for Tissue Engineering* (Eds: S. Thomas, Y. Grohens, N. Ninan), Elsevier, Amsterdam **2015**, p. 45–55.
[53] S. Suresh, A. Becker, B. Glasmacher, *Polymers* **2020**, *12*, 2448.
[54] A. H. Hekmati, A. Rashidi, R. Ghazisaeidi, J.-Y. Drean, *Text. Res. J.* **2013**, *83*, 1452.
[55] S. Shi, Y. Si, Y. Han, T. Wu, M. I. Iqbal, B. Fei, R. K. Y. Li, J. Hu, J. Qu, *Adv. Mater.* **2022**, *34*, 2107938.
[56] S. M. Feng, X. L. Liu, J. Qi, D. L. Huang, Z. C. Xiong, *Mater. Res. Express* **2019**, *6*, 125330.
[57] A. Koski, K. Yim, S. Shivkumar, *Mater. Lett.* **2004**, *58*, 493.
[58] J. Avossa, G. Herwig, C. Toncelli, F. Itel, R. M. Rossi, *Green Chem.* **2022**, *24*, 2347.
[59] C. J. Angammana, S. H. Jayaram, *IEEE Trans. Ind. Appl.* **2011**, *47*, 1109.
[60] A. S. Levitt, R. Vallett, G. Dion, C. L. Schauer, *J. Appl. Polym. Sci.* **2018**, *135*, 46404.
[61] A. Dodero, E. Brunengo, M. Alloisio, A. Sionkowska, S. Vicini, M. Castellano, *Carbohydr. Polym.* **2020**, *235*, 115976.
[62] S. Kailasa, M. S. B Reddy, M. R. Maurya, B. G Rani, K. V Rao, K. K. Sadasivuni, *Macromol. Mater. Eng.* **2021**, *306*, 2100410.
[63] G. K. Sharma, N. R. James, in *Recent Developments in Nanofibers Research* (Eds: M. Khan, S. J. Samuel Chelladurai), IntechOpen, London **2022**.
[64] N. Amariei, L. R. Manea, A. P. Bertea, A. Bertea, A. Popa, *IOP Conf. Ser.: Mater. Sci. Eng.* **2017**, *209*, 012092.
[65] A. Raksa, P.-O. Numpaisal, Y. Ruksakulpiwat, *Mater. Today* **2021**, *47*, 3458.
[66] G.-Z. Yang, H.-P. Li, J.-H. Yang, J. Wan, D.-G. Yu, *Nanoscale Res. Lett.* **2017**, *12*, 55.
[67] K. Valachová, M. A. El Meligy, L. Šoltés, *Int. J. Biol. Macromol.* **2022**, *206*, 74.
[68] A. D. J. Bombin, N. J. Dunne, H. O. McCarthy, *Mater. Sci. Eng., C* **2020**, *114*, 110994.
[69] W. Peng, D. Li, K. Dai, Y. Wang, P. Song, H. Li, P. Tang, Z. Zhang, Z. Li, Y. Zhou, C. Zhou, *Int. J. Biol. Macromol.* **2022**, *208*, 400.
[70] S. Homaeigohar, A. R. Boccaccini, *Acta Biomater.* **2020**, *107*, 25.
[71] J. X. Law, L. L. Liau, A. Saim, Y. Yang, R. Idrus, *Tissue Eng. Regener. Med.* **2017**, *14*, 699.
[72] P. Li, L. Ruan, R. Wang, T. Liu, G. Song, X. Gao, G. Jiang, X. Liu, *J. Bionic Eng.* **2021**, *18*, 1378.
[73] A. Gaspar-Pintiliescu, A.-M. Stanciuc, O. Craciunescu, *Int. J. Biol. Macromol.* **2019**, *138*, 854.
[74] C. E. Campiglio, N. Contessi Negrini, S. Farè, L. Draghi, *Materials* **2019**, *12*, 2476.
[75] T. Li, M. Sun, S. Wu, *Nanomaterials* **2022**, *12*, 784.
[76] S. Ullah, X. Chen, *Appl. Mater. Today* **2020**, *20*, 100656.
[77] H. Xiao, X. Chen, X. Liu, G. Wen, Y. Yu, *Mater. Today Bio* **2023**, *19*, 100589.
[78] L. Baumann, E. F. Bernstein, A. S. Weiss, D. Bates, S. Humphrey, M. Silberberg, R. Daniels, *Aesthetic Surg. J. Open Forum* **2021**, *3*, ojab019.
[79] S. Khalili, S. N. Khorasani, S. M. Razavi, B. Hashemibeni, A. Tamayol, *Appl. Biochem. Biotechnol.* **2019**, *187*, 1193.
[80] G. Sandri, S. Rossi, M. C. Bonferoni, D. Miele, A. Faccendini, E. Del Favero, E. Di Cola, A. I. Cornaglia, C. Boselli, T. Luxbacher, L. Malavasi, L. Cantu', F. Ferrari, *Carbohydr. Polym.* **2019**, *220*, 219.
[81] S. Su, T. Bedir, C. Kalkandelen, A. Ozan Basar, H. Turkoglu Sasmazel, C. Bulent Ustundag, M. Sengor, O. Gunduz, *Eur. Polym. J.* **2021**, *142*, 110158.
[82] H. Hosseini, M. K. Shahraky, A. Amani, F. S. Landi, *Polym. Adv. Technol.* **2021**, *32*, 574.
[83] S. Jiang, Y. Zhuang, M. Cai, X. Wang, K. Lin, *Eng. Regener.* **2023**, *4*, 357.
[84] F. Yu, A. U. R. Khan, H. Zheng, X. Li, M. EL-Newehy, H. EL-Hamshary, Y. Morsi, J. Li, J. Wu, X. Mo, *Colloids Surf., B* **2022**, *217*, 112691.
[85] Pu Luo, R. Huang, Y. Wu, X. Liu, Z. Shan, Li Gong, S. Deng, H. Liu, J. Fang, S. Wu, X. Wu, Q. Liu, Z. Chen, K. W. K. Yeung, W. Qiao, S. Chen, Z. Chen, *Bioact. Mater.* **2023**, *28*, 95.
[86] H. H. Elmashhady, B. A. Kraemer, K. H. Patel, S. A. Sell, K. Garg, *Electrospinning* **2017**, *1*, 87.
[87] H.-S. Kim, H.-J. Hwang, H.-J. Kim, Y. Choi, D. Lee, H.-H. Jung, S. H. Do, *Front. Bioeng. Biotechnol.* **2022**, *10*, 865545.
[88] S. Ahmadian, M. Ghorbani, F. Mahmoodzadeh, *Int. J. Biol. Macromol.* **2020**, *162*, 1555.
[89] P. Sobhanian, M. Khorram, S.-S. Hashemi, A. Mohammadi, *Int. J. Biol. Macromol.* **2019**, *130*, 977.
[90] J. Hou, L. Chen, Z. Liu, J. Li, J. Yang, A. Zhong, M. Zhou, Y. Sun, L. Guo, Y. Yang, J. Sun, Z. Wang, *J. Biomed. Mater. Res., Part A* **2019**, *107*, 1414.
[91] A. Hivechi, S. H. Bahrami, R. A. Siegel, P. B. Milan, M. Amoupour, *Cellulose* **2020**, *27*, 5179.
[92] A. Jafari, A. Amirsadeghi, S. Hassanajili, N. Azarpira, *Int. J. Pharm.* **2020**, *583*, 119413.
[93] A. Li, L. Li, B. Zhao, X. Li, W. Liang, M. Lang, B. Cheng, J. Li, *Int. J. Biol. Macromol.* **2022**, *194*, 914.
[94] J. Maitz, Y. Wang, A. Fathi, F. X. Escobar, R. Parungao, P. van Zuijlen, P. Maitz, Z. Li, *J. Tissue Eng. Regener. Med.* **2020**, *14*, 1189.
[95] J. J. Vázquez, E. S. M. Martínez, *J. Mater. Res.* **2019**, *34*, 2819.
[96] A. Bryan, E. Wales, S. Vedante, A. Blanquer, D. Neupane, S. Mishra, L. Backová, T. Fujiwara, J. A. Jennings, J. D. Bumgardner, *Mar. Drugs* **2022**, *20*, 615.
[97] G. Chen, J. Guo, J. Nie, G. Ma, *Polymer* **2016**, *83*, 12.
[98] M. R. El-Aassar, N. G. El-Beheri, M. M. Agwa, H. M. Eltaher, M. Alseqely, W. S. Sadik, L. El-Khordagui, *Int. J. Biol. Macromol.* **2021**, *167*, 1552.
[99] A. Chanda, J. Adhikari, A. Ghosh, S. R. Chowdhury, S. Thomas, P. Datta, P. Saha, *Int. J. Biol. Macromol.* **2018**, *116*, 774.
[100] D. R. Figueira, S. P. Miguel, K. D. de Sá, I. J. Correia, *Int. J. Biol. Macromol.* **2016**, *93*, 1100.

[101] X. Zhang, R. Lv, L. Chen, R. Sun, Y. Zhang, R. Sheng, T. Du, Y. Li, Y. Qi, *ACS Appl. Mater. Interfaces* **2022**, *14*, 12984.
[102] M. Khandaker, H. Nomhwange, H. Progri, S. Nikfarjam, M. B. Vaughan, *Bioengineering* **2022**, *9*, 19.
[103] S. Stojanov, A. Berlec, *Front. Bioeng. Biotechnol.* **2020**, *8*, 130.
[104] L. Bacakova, M. Zikmundova, J. Pajorova, A. Broz, E. Filova, A. Blanquer, R. Matejka, J. Stepanovska, P. Mikes, V. Jencova, E. Kuzelova Kostakova, A. Sinica, *Applications of Nanobiotechnology* (Eds: M. Stoytcheva, R. Zlatey), IntechOpen, London **2019**.
[105] H. Maleki, B. Azimi, S. Ismaeilimoghadam, S. Danti, *Appl. Sci.* **2022**, *12*, 3192.
[106] M. Santoro, S. R. Shah, J. L. Walker, A. G. Mikos, *Adv. Drug Delivery Rev.* **2016**, *107*, 206.
[107] M. A. Teixeira, M. T. P. Amorim, H. P. Felgueiras, *Polymers* **2019**, *12*, 7.
[108] J.-C. Park, T. Ito, K-Oh Kim, K.-W. Kim, B.-S. Kim, M.-S. Khil, H.-Y. Kim, I.-S. Kim, *Polym. J.* **2010**, *42*, 273.
[109] D. Essa, P. P. D. Kondiah, Y. E. Choonara, V. Pillay, *Front. Bioeng. Biotechnol.* **2020**, *8*, 48.
[110] F. S. Tabatabaei Mirakabad, K. Nejati-Koshki, A. Akbarzadeh, M. R. Yamchi, M. Milani, N. Zarghami, V. Zeighamian, A. Rahimzadeh, S. Alimohammadi, Y. Hanifehpour, S. W. Joo, *Asian Pac. J. Cancer Prev.* **2014**, *15*, 517.
[111] S. Fahimirad, H. Abtahi, P. Satei, E. Ghaznavi-Rad, M. Moslehi, A. Ganji, *Carbohydr. Polym.* **2021**, *259*, 117640.
[112] M. A. Norouzi, M. Montazer, T. Harifi, P. Karimi, *Polym. Test.* **2021**, *93*, 106914.
[113] Y. Agarwal, P. S. Rajinikanth, S. Ranjan, U. Tiwari, J. Balasubramnaiam, P. Pandey, D. K. Arya, S. Anand, P. Deepak, *Int. J. Biol. Macromol.* **2021**, *176*, 376.
[114] L. Moradkhannejhad, M. Abdouss, N. Nikfarjam, M. H. Shahriari, V. Heidary, *J. Drug Delivery Sci. Technol.* **2020**, *56*, 101554.
[115] H. Bi, T. Feng, B. Li, Y. Han, *Polymers* **2020**, *12*, 839.
[116] T. Fan, R. Daniels, *AAPS PharmSciTech* **2021**, *22*, 1.
[117] T.-Y. Huang, G.-S. Wang, C.-C. Tseng, W.-T. Su, *Mater. Sci. Eng., C* **2019**, *104*, 109986.
[118] H. Oh, D. Son, J. S. Lee, M. Kim, D. Sung, H. Lee, W. Il Choi, *Int. J. Biol. Macromol.* **2022**, *219*, 835.
[119] N. Eghbalifam, S. A. Shojaosadati, S. Hashemi-Najafabadi, A. C. Khorasani, *Int. J. Biol. Macromol.* **2020**, *155*, 119.
[120] C.-H. Lee, C.-H. Huang, K.-C. Hung, S.-C. Huang, C.-C. Kuo, S.-J. Liu, *Pharmaceuticals* **2022**, *15*, 1358.
[121] C.-H. Lee, D.-Y. Chen, M.-J. Hsieh, K.-C. Hung, S.-C. Huang, C.-J. Cho, S.-J. Liu, *Front. Bioeng. Biotechnol.* **2023**, *11*, 1075720.
[122] H. T. Liao, Y.-T. Lai, C.-Y. Kuo, J.-P. Chen, *Mater. Sci. Eng., C* **2021**, *120*, 111689.
[123] X. Chen, H. Cao, Y. He, Q. Zhou, Z. Li, W. Wang, Y. He, G. Tao, C. Hou, *Front. Optoelectron.* **2022**, *15*, 50.
[124] Z. Mbese, S. Alven, B. A. Aderibigbe, *Polymers* **2021**, *13*, 4368.
[125] D. D. Akolpoglu Basaran, U. Gündüz, A. Tezcaner, D. Keskin, *Int. J. Pharm.* **2021**, *597*, 120207.
[126] T. Selvaras, S. A. Alshamrani, R. Gopal, S. K. Jaganathan, S. Sivalingam, S. Kadiman, S. Saidin, *J. Biomed. Mater. Res., Part B* **2023**, *111*, 1171.
[127] M. Ghorbani, P. Nezhad-Mokhtari, S. Ramazani, *Int. J. Biol. Macromol.* **2020**, *153*, 921.
[128] A. V. Nguyen, A. M. Soulika, *Int. J. Mol. Sci.* **2019**, *20*, 1811.
[129] P. Krzyszczyk, R. Schloss, A. Palmer, F. Berthiaume, *Front. Physiol.* **2018**, *9*, 419.
[130] J. Mao, Lu Chen, Z. Cai, S. Qian, Z. Liu, B. Zhao, Y. Zhang, X. Sun, W. Cui, *Adv. Funct. Mater.* **2022**, *32*, 2111003.
[131] M. Kloc, R. M. Ghobrial, J. Wosik, A. Lewicka, S. Lewicki, J. Z. Kubiak, *J. Tissue Eng. Regener. Med.* **2019**, *13*, 99.
[132] C. Yunna, Hu Mengru, W. Lei, C. Weidong, *Eur. J. Pharmacol.* **2020**, *877*, 173090.
[133] Y. Yao, X.-H. Xu, L. Jin, *Front. Immunol.* **2019**, *10*, 792.
[134] K. Y. Lee, *Med. Biol. Sci. Eng.* **2019**, *2*, 1.
[135] L. Chang-Hoon, C. E Young, *J. Rheum. Dis.* **2018**, *25*, 11.
[136] S. Khan, M. Ruutu, R. Thomas, N. Bhardwaj, in *Kelley's Textbook of Rheumatology* (Eds: G. S. Firestein, R. C. Budd, S. E. Gabriel, I. B. McInnes, J. R. O'Dell, W. N. Kelley), Elsevier, Philadelphia, PA **2013**, p. 117.
[137] O. Stojadinovic, N. Yin, J. Lehmann, I. Pastar, R. S. Kirsner, M. Tomic-Canic, *Immunol Res* **2013**, *57*, 222.
[138] K. Clayton, A. F. Vallejo, J. Davies, S. Sirvent, M. E. Polak, *Front. Immunol.* **2017**, *8*, 1676.
[139] A. C. G. Salina, N. Klopfenstein, J. Pinon, C. Henrique Serezani, in *Macrophages in the Human Body: A Tissue Level Approach* (Eds: N. O. Saraiva Camara, T. Teodoro Braga), Academic Press, London **2022**, p. 139.
[140] M. T. Ochoa, A. Loncaric, S. R. Krutzik, T. C. Becker, R. L. Modlin, *J. Invest. Dermatol.* **2008**, *128*, 2225.
[141] S. P. Shankar, *World J. Immunol.* **2015**, *5*, 113.
[142] M. Vinish, W. Cui, E. Stafford, L. Bae, H. Hawkins, R. Cox, T. Toliver-Kinsky, *Wound Repair Regener.* **2016**, *24*, 6.
[143] J. Aron-Wisnewsky, J. Tordjman, C. Poitou, F. Darakhshan, D. Hugol, A. Basdevant, A. Aissat, M. Guerre-Millo, K. Clément, *J. Clin. Endocrinol. Metab.* **2009**, *94*, 4619.
[144] W. Liang, Y. Qi, H. Yi, C. Mao, Q. Meng, H. Wang, C. Zheng, **2022**, *13*, 908749.
[145] I. Shaked, D. B. Hanna, C. Gleißner, B. Marsh, J. Plants, D. Tracy, K. Anastos, M. Cohen, E. T. Golub, R. Karim, J. Lazar, V. Prasad, P. C. Tien, M. A. Young, A. L. Landay, R. C. Kaplan, K. Ley, *Arterioscler., Thromb., Vasc. Biol.* **2014**, *34*, 1085.
[146] N. Fujiwara, K. Kobayashi, *Curr. Drug Targets: Inflammation Allergy* **2005**, *4*, 281.
[147] L. C. Davies, S. J. Jenkins, J. E. Allen, P. R. Taylor, *Nat. Immunol.* **2013**, *14*, 986.
[148] Y. Wu, K. K. Hirschi, *Front. Cell Dev. Biol.* **2021**, *8*, 617879.
[149] S. M. Millard, O. Heng, K. S. Opperman, A. Sehgal, K. M. Irvine, S. Kaur, C. J. Sandrock, A. C. Wu, G. W. Magor, L. Batoon, A. C. Perkins, J. E. Noll, A. C. W. Zannettino, D. P. Sester, J.-P. Levesque, D. A. Hume, L. J. Raggatt, K. M. Summers, A. R. Pettit, *Cell Rep.* **2021**, *37*, 110058.
[150] Y. Jia, W. Yang, K. Zhang, S. Qiu, J. Xu, C. Wang, Y. Chai, *Acta Biomater.* **2019**, *83*, 291.
[151] L. Irsay, P. Mandl, P. V. Balint, R. J. Wakefield, M. A. D'Agostino, in *Essential Applications of Musculoskeletal Ultrasound in Rheumatology* (Eds: R. Wakefield, M. A. D'Agostino), Saunders Elsevier, Philadelphia **2010**.
[152] Y. Ren, Yi Chen, W. Chen, H. Deng, P. Li, Y. Liu, C. Gao, G. Tian, C. Ning, Z. Yuan, X. Sui, S. Liu, Q. Guo, *J. Nanobiotechnol.* **2023**, *21*, 269.
[153] J. Huang, X. Zhou, Y. Shen, H. Li, G. Zhou, W. Zhang, Y. Zhang, W. Liu, *J. Biomed. Mater. Res., Part A* **2020**, *108*, 69.
[154] J. R. Nakkala, Y. Yao, Z. Zhai, Y. Duan, D. Zhang, Z. Mao, L. Lu, C. Gao, *Small* **2021**, *17*, 2006992.
[155] J. Xie, X. Wu, S. Zheng, K. Lin, J. Su, *J. Nanobiotechnol.* **2022**, *20*, 342.
[156] C. Wang, C. Chu, X. Zhao, Y. Yang, C. Hu, Li Liu, J. Li, Y. Qu, Yi Man, *Bioact. Mater.* **2022**, *11*, 206.
[157] Z. Zhu, Y. Liu, Y. Xue, X. Cheng, W. Zhao, J. Wang, R. He, Q. Wan, X. Pei, *ACS Appl. Mater. Interfaces* **2019**, *11*, 36141.
[158] J. R. Nakkala, Y. Duan, J. Ding, W. Muhammad, D. Zhang, Z. Mao, H. Ouyang, C. Gao, *Acta Biomater.* **2022**, *141*, 24.
[159] K. T. Kurpinski, J. T. Stephenson, R. R. R. Janairo, H. Lee, S. Li, *Biomaterials* **2010**, *31*, 3536.

[160] T. Zhang, Z. Xiang, L. Liu, Z. Ma, M. Panteleev, F. I. Ataullakhanov, Q. Shi, *Macromol. Biosci.* **2023**, *23*, 2300036.
[161] M. Bessa-Gonçalves, C. Ribeiro-Machado, M. Costa, Cc Ribeiro, Jn Barbosa, Ma Barbosa, Sg Santos, *Acta Biomater.* **2023**, *155*, 667.
[162] S. Liu, L. Yao, Y. Wang, Yi Li, Y. Jia, Y. Yang, Na Li, Y. Hu, D. Kong, X. Dong, K. Wang, M. Zhu, *Bioact. Mater.* **2023**, *21*, 464.
[163] S. Chen, A. F. U. H. Saeed, Q. Liu, Q. Jiang, H. Xu, G. G. Xiao, L. Rao, Y. Duo, *Signal Transduction Targeted Ther.* **2023**, *8*, 207.
[164] M. Liu, W. Zhang, Z. Chen, Y. Ding, B. Sun, H. Wang, X. Mo, J. Wu, *J. Biomed. Mater. Res., Part A* **2023**, *111*, 132.
[165] Y. Niu, F. J. Stadler, Xu Yang, F. Deng, G. Liu, H. Xia, *J. Nanobiotechnol.* **2021**, *19*, 283.
[166] M. B. Taskin, T. Tylek, C. Blum, C. Böhm, C. Wiesbeck, J. Groll, *ACS Biomater. Sci. Eng.* **2021**, *7*, 3166.
[167] J. Liu, T. Li, H. Zhang, W. Zhao, L. Qu, S. Chen, S. Wu, *Mater. Today Bio* **2022**, *14*, 100243.
[168] H. Yu, Y. Li, Y. Pan, H. Wang, W. Wang, X. Ren, H. Yuan, Z. Lv, Y. Zuo, Z. Liu, W. Lin, Q. Yao, *J. Nanobiotechnol.* **2023**, *21*, 110.
[169] M. Ryma, T. Tylek, J. Liebscher, C. Blum, R. Fernandez, C. Böhm, W. Kastenmüller, G. Gasteiger, J. Groll, *Adv. Mater.* **2021**, *33*, 2101228.
[170] S. Gao, T. Chen, Z. Wang, P. Ji, L. Xu, W. Cui, Y. Wang, *J. Nanobiotechnol.* **2022**, *20*, 294.
[171] D. Zhang, L. Li, Y. Shan, J. Xiong, Z. Hu, Y. Zhang, J. Gao, *J. Drug Delivery Sci. Technol.* **2019**, *52*, 272.
[172] J. He, Y. Liang, M. Shi, B. Guo, *Chem. Eng. J.* **2020**, *385*, 123464.
[173] R.-X. Wu, C. Ma, Y. Liang, F.-M. Chen, X. Liu, *Appl. Mater. Today* **2020**, *18*, 100508.
[174] Lu Chen, L. Zhang, H. Zhang, X. Sun, D. Liu, J. Zhang, Y. Zhang, L. Cheng, H. A. Santos, W. Cui, *Bioact. Mater.* **2021**, *6*, 3218.
[175] G. Zhong, M. Qiu, J. Zhang, F. Jiang, X. Yue, C. Huang, S. Zhao, R. Zeng, C. Zhang, Y. Qu, *Int. J. Biol. Macromol.* **2023**, *234*, 123693.
[176] M. Sheikholeslam, M. E. E. Wright, N. Cheng, H. Hee Oh, Y. Wang, A. K. Datu, J. Paul Santerre, S. Amini-Nik, M. G. Jeschke, *ACS Biomater. Sci. Eng.* **2019**, *6*, 505.
[177] F. Zhou, S. Sun, C. Cui, X. Li, S. Wu, J. Ma, S. Chen, C. M. Li, *Int. J. Biol. Macromol.* **2023**, *253*, 127086.
[178] H. Zhang, M. Zhang, X. Wang, Mi Zhang, X. Wang, Y. Li, Z. Cui, X. Chen, Y. Han, W. Zhao, *Drug Delivery* **2022**, *29*, 174.
[179] I. H. Ali, A. Ouf, F. Elshishiny, M. B. Taskin, J. Song, M. Dong, M. Chen, R. Siam, W. Mamdouh, *ACS Omega* **2022**, *7*, 1838.
[180] A. Eskandarinia, A. Kefayat, M. Agheb, M. Rafienia, M. Amini Baghbadorani, S. Navid, K. Ebrahimpour, D. Khodabakhshi, F. Ghahremani, *Sci. Rep.* **2020**, *10*, 3063.
[181] N. Jirofti, M. Golandi, J. Moyaffagh, F. Shahriari Ahmadi, F. Kalalinia, *ACS Biomater. Sci. Eng.* **2021**, *7*, 3886.
[182] G. Ramanathan, S. Singaravelu, M. D. Raja, N. Nagiah, P. Padmapriya, K. Ruban, K. Kaveri, T. S. Natarajan, U. Tiruchirapalli Sivagnanam, P. Thirumalai Perumal, *RSC Adv.* **2016**, *6*, 7914.
[183] A. Z. Bazmandeh, E. Mirzaei, M. Fadaie, S. Shirian, Y. Ghasemi, *Int. J. Biol. Macromol.* **2020**, *162*, 359.
[184] P. Chandika, F. Khan, S.-Y. Heo, Y.-M. Kim, M. Yi, W.-K. Jung, *Biomater. Adv.* **2022**, *140*, 213046.
[185] Z. Hadisi, M. Farokhi, H. R. Bakhsheshi-Rad, M. Jahanshahi, S. Hasanpour, E. Pagan, A. Dolatshahi-Pirouz, Y. S. Zhang, S. C. Kundu, M. Akbari, *Macromol. Biosci.* **2020**, *20*, 1900328.
[186] S. Y. Lee, S. Jeon, Y. W. Kwon, M. Kwon, M. S. Kang, K.-Y. Seong, T.-E. Park, S. Y. Yang, D.-W. Han, S. W. Hong, K. S. Kim, *Sci. Adv.* **2022**, *8*, abn1646.

Hyeonseo Park is a Master's student in Biosystems Engineering at Kangwon National University, South Korea. Her research interest is macrophage polarization and guided wound healing using nanofiber scaffolds through an electrospinning technique.

Tejal V. Patil is a Ph.D. student of Biosystems Engineering at Kangwon National University, South Korea. She received her Master's degree from the Institute of Chemical Technology, Mumbai, India. Her research interest is developing stuimuli responsive biomaterials for application in bacteria eradication and tissue regeneration.

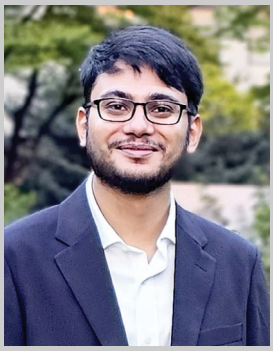

Sayan Deb Dutta is a postdoctoral research associate at Kangwon National University. He received his Doctoral degree from the Department of Biosystems Engineering at Kangwon National University, South Korea. He reviewed his Master's degree from the University of Kalyani, India. His research interest is the synthesis of multifunctional nanomaterials for 3D printing and nanotheranostic applications for tissue engineering.

Jieun Lee is a Master's student in Biosystems Engineering at Kangwon National University, South Korea. Her research is the development of various conductive 3D hydrogels for tissue regeneration and healing.

Keya Ganguly is a postdoctoral research associate at Kangwon National University. She received her Doctoral degree from the Department of Biosystems Engineering at Kangwon National University, South Korea. She received her Master's degree from Presidency University, India. Her research interest is developing a multi-stimuli-assisted scaffolding platform for tissue engineering and biosensing.

Aayushi Randhawa is a doctoral student in Biosystems Engineering at Kangwon National University, South Korea. She received her Master's degree from Bangalore University, India. Her research interest is the synthesis of 3D-printed structures for the healing and regeneration of damaged bone tissues.

Hojin Kim is a Master's student in Biosystems Engineering at Kangwon National University, South Korea. His research interest is Nanocellulose hydrogel for wound healing and sensing.

Ki-Taek Lim is a professor at the Department of Biosystems Engineering at Kangwon National University, South Korea. He received his Doctoral degree from Seoul National University, South Korea, and joined as a postdoctoral research fellow at the University of Arkansas, USA. He has a strong knowledge of mechatronics and regenerative medicines. His research focuses on developing the bio-nanorobotics system with novel bioreactors and stem cell cultures for tissue-engineering applications.